POLITECNICO
MILANO 1863

SCUOLA DI INGEGNERIA INDUSTRIALE
E DELL'INFORMAZIONE

Analysis of the conservation of sliding mesh algorithms dealing with non-planar interfaces.

Tesi di Laurea Magistrale in
Aeronautical Engineering - Ingegneria Aeronautica

Davide Mazzucchetti, 10539948

Advisor:
Barbara Re

Co-advisors:
Dr. Giulio Gori

Academic year:
2022-2023

Abstract: The aim of the present study is to investigate whether three different sliding mesh techniques, namely nearest neighbor, isoparametric, and weighted average, can introduce errors in the conservation of flow properties when dealing with non-planar interfaces. The analysis is conducted by comparing the three approach, and by evaluating the influence of the type of grid discretization on the conservation errors. For this purpose, four different cases with increasing flow complexity are examined, beginning with a uniform flow and concluding with a flow that exhibits discontinuities such as a shock wave. The performance of these approaches will then be evaluated by verifying both the conservation of global quantities and the preservation of flow characteristics. These three techniques turn out to be non conservatives since they all introduce errors in the mass and total energy in the domain. Moreover they generate oscillations in the flow variables at the interface which are then propagated in the rest of the domain.

Key-words: sliding mesh, non-conforming grid, non-planar grid interfaces, unstructured finite volume scheme

1. Introduction

Unsteady CFD simulations frequently need to adjust the computational domain to accommodate the movement of the simulated object or the deformation of its surfaces. Dynamic grid methods can be used to accurately follow small grid deformation by maintaining the grid connectivity fixed, updating only the nodes position. These strategies though, cannot be used with arbitrarily large displacement.
One potential approach to address this scenario involves the division the computational domain into different zones that can be set in motion relative to each other. This partition enables the use of distinct space discretization for each block, being able to address phenomena with varying characteristic scales. This is the idea underlying the so called Chimera method[1, 2]. The governing equations are solved independently for each mesh block, and to reconcile the solutions, an overlapping background grid is employed. The solution variables are then interpolated between the two grids. However, this procedure does not guarantee the scheme to be conservative. If mass, momentum, and energy are not conserved across the interface, problems may arise in the case of discontinuity propagation, leading to non-physical solutions.
Another possible technique is represented by the so-called *Sliding Meshes*. In this approach the domain is still subdivided into different zones but in this case, neither gaps or overlaps between the different sub-domains are allowed. The conservation of the flow properties though remains a non trivial task.

One of the initial ideas to conserve the flow properties at the interface was introduced by Berger[3]. Nearly simultaneously M. Rai[4] developed a conservative zonal-boundary scheme, consisting in the interface splitting into conformal sub-grids. This technique though, works only with planar interfaces, which turns out to be difficult to achieve in many cases.
Another approach to deal with non conformal interface has been presented by Lerat and Wu[5]: their main idea was to split the interface edges into smaller elements and to compute the numerical fluxes on them. The numerical fluxes are then summed, without using an interpolation step.
Another idea used to achieve conservation consists in the use of new local mesh at the interfaces, as described by Behr and Tezduyar[6], where the local mesh is presented as a thin layer of deforming element.
Other approaches, instead, are based on the idea of a *supermesh* used as an auxiliary mesh to create a new connectivity between the interface grid. This idea was first introduced by Farrel et al.[7] and then used also by Rinaldi et al.[8]. The key concept of this last approach will be briefly described in sec. 2.3.
Lastly, a completely different method relies on local mesh adaptation techniques. The mesh quality can be restored by node deletion, node swapping and node insertion. Recently, Guardone, Isola Re and co-authors[9–11] proposed a strategy to describe these adaptations within the arbitrary Lagrangian-Eulerian (ALE) formulation avoiding the use of any interpolation and ensuring conservation.
The aim of this article is to study the error introduced by three methods implemented in the SU2[12] framework (Nearest Neighbor, Isoparametric and Weighted Average) used to deal with the sliding meshes in the case of non-rectilinear interfaces. In particular the analysis focuses on the conservation of the proposed methods, on their compare and the influence that the grid discretization can have on them.
Firstly, in sec 2 a brief description of the tested algorithms is provided. Then the analysis starts from the simplest case, the so-called free-stream preservation, described in sec 4. The complexity of the flow field is then progressively increased in the sections 5-6-7. The conclusions of this work are presented in sec 8.

2. SU2 Algorithms

SU2 is an open-source Computational Fluid Dynamics (CFD) software designed for solving partial differential equations (PDE). SU2 is also capable of performing multi-zone simulations since three different algorithms are already implemented in its framework. The techniques implemented in SU2 employed for this purpose and analysed in this paper are:

- Nearest Neighbor
- Isoparametric
- Weighted Average

In order to conduct this type of simulations the program must be able to transfer the information of the flow variables from one zone to the other. The procedure for doing this kind of computations is shared by all the methods implemented. In general, this routine is characterized by the subdivision of the domain into *donor zones* and *target zones*.
The donor zone is needed to define which of the two sides of an interface is the starting point for the information transfer. On the other hand the target zone represents the zone that will receive the information. A brief description of how these methods work is provided in the following paragraphs.

2.1. Nearest Neighbor

Nearest neighbor (NN) is the first technique considered here; this is the simplest and the theoretically less accurate one. This approach consists in the identification of the nearest donor point for every target node; the choice of this point is based on the Euclidean distance between them. Then the information from the closest donor point is simply transferred to the target one. With this approach is clear that the distribution of the nodes on the two sides of the interface has a significant impact on the results and errors can arise if the distance between donor and target nodes is large.

2.2. Isoparametric

The second technique analysed in this work is the so called *Isoparametric* (ISO). In this method the interpolation is performed by searching, for every target, the two nearest donor points. Then, in order for the interpolation to be conducted, two isoparametric coefficients are needed. These coefficients are calculated by projecting the target node onto the line connecting the two donor nodes. The distances between the projected point and each donor node are then computed and utilized to determine the interpolation weights. Consequently, donor nodes in closer proximity have a more significant influence on the interpolation results compared to those located

farther away. Since this method relies on more than just one node to perform the information transfer, it is expected to be less sensitive on the nodes distribution with respect to the previous one.

2.3. Weighted Average

The third algorithm considered here is the *Weighted Average* (WA), based on the approach introduced by Rinaldi et al. [8]. The effectiveness of this method in ensuring flux conservation has been previously demonstrated in the context of rectilinear interfaces. The efficacy over curved sliding grid instead still have to be investigated.
The key idea of this method is the construction of a *supermesh* layer between the two touching grids in order to establish a new connectivity between the two meshes. Once the new grid layer is created it is used to compute the numerical fluxes, which will be then added to the flux balance of the control volumes of the initial grids.
In the SU2 framework the supermesh construction is implemented as follows: initially, for each target node, the nearest donor point is identified. The supermesh is then generated near the target point and subsequently expanded in all directions, incorporating donor elements that are in proximity to the initial donor node. This process continues until the entire interface is completely covered.

3. Test Cases

In order to assess the influence of the grid on the conservation and the differences between each method, four different cases are tested. These tests are presented starting from the simplest one and then increasing progressively the complexity of the flow field.
The first case analysed consists in the simulation of a free-stream subsonic flow which enters and leaves the computational domain without any interaction. The idea underlying this test is to see if the quantities in the domain, like mass and total energy, are conserved even if the domain is dividing into two zones and one of them is rotating.
The focus of the analysis is then shifted to a more complex case, consisting in two circular crowns sharing the same center. The flow enters the domain from the inner circumference and exits from the external one. In this scenario the flow is no more uniform but presents spatial gradients. This allows to study the differences in the behaviour of the three techniques.
The last two tests are used to assess the capabilities of the sliding mesh to preserve the flow characteristics. The third case represents an inviscid vortex, governed by compressible Euler equations, which is advected by the mean flow. During the advection the vortex crosses the interface between two zones. Theoretically the vortex properties should be constant throughout its movement and, if these techniques were conservatives, no errors should be introduced.
The last test consists in a flow with a sharp discontinuity such as a shock wave. An oblique shock is created and it develops through a rotating zone. This last case is used to check if the mass and the total energy are conserved during the simulation and to see if spurious oscillations arise at the interface.

4. Free Stream Conservation

The analysis of the conservation capabilities of the three techniques previously described starts from the simplest scenario: the free-stream preservation of a subsonic flow. For this test 5 different kinds of grid were used: first of all, a simulation using one single zone is conducted. The domain is a rectangle with dimensions $[-2, 2] \times [-1, 1]$, inviscid wall boundary conditions are applied on the upper and lower boundary while the left and the right boundary are set as farfield. The Mach number of the flow is set to $M = 0.05$, the pressure and the temperature of the undisturbed flow are respectively $P = 101325Pa$, $T = 273.15K$.
The simulations in the multi-zone case instead were run using an external rectangular grid having the same dimensions of the previous one with a hole in the middle: the internal zone is a circle with radius $r = 0.5$. The discretization of the external grid was the same for all the simulations; the internal one is refined dividing the size of the element by 2, 3, 4. Fig. 1 shows has an example the grid for the case of interface with 1/2 ratio.

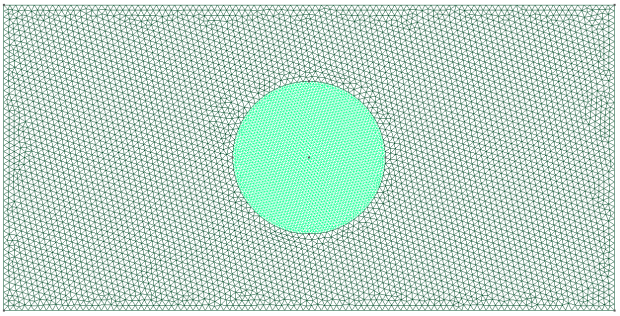

Figure 1: Example of a mesh for the free-stream preservation test. In this case, the elements of the internal grid are half the size of those of the external zone.

Two different kind of simulations were performed: keeping the internal grid fixed and making the internal zone rotate about its centre. The flow goes from left to right and since the simulation is steady the mass flux entering in the domain from the left boundary is equal to the flux that leaves the domain on the right side. This means that, if conservation is achieved, the mass and the total energy in the domain must stay constant.
To check the conservativity of the proposed methods, the integrals over the domain of the density and of the total energy have been computed using the mid point rule. So this first test is carried out by running 25 simulations:

- 1 single zone simulation
- 12 simulations(3 techniques for each of the four mesh configuration) keeping the internal zone fixed
- 12 simulations with rotating internal zone

As expected, in the first simulation the conservation is perfectly achieved, the total value of mass and energy in the domain is exactly the same after every time step.
In the multi-zone simulations problems could arise at the interface due to the presence of the so called *hanging nodes*. This expression refers to nodes of the internal zone that lie inside an element of the external one instead of being on the edge of the element and vice-versa. This happens because of the different discretization on the two sides of the interface. Despite this fact the conservation is obtained also in the case with two fixed zone: no error showed up neither in the mass nor in the energy for all the three methods and with every kind of interface. This means that the methods implemented in SU2 are capable of transferring information without any loss even if the interface presents non conformal grid, if the two zones are kept fixed.
When one of the zone rotates an error both in the mass and in the energy is generated.

	WA	**NN**	**ISO**
1:1	$7.056E-15$	$7.056E-15$	$7.056E-15$
1:2	$7.056E-15$	$7056E-15$	$7.056E-15$
1:3	$7.056E-15$	$7.056E-15$	$7056E-15$
1:4	$7.056E-15$	$7.056E-15$	$7.056E-15$

Table 1: Uniform flow: In this table are shown the average values of the error associated to the conservation of mass after every iteration in the case of rotating internal zone. Since the flow is uniform there is no difference between the three methods. Moreover the type of grid discretization has no influence on the conservation error. The errors associated to the total energy show the same behaviour and order of magnitude and thus are not reported here.

As clearly visible in tab. 1 the average value of the error per iteration in this case is small and close to machine precision, but the fact that is present means that there might be any loss when two interface are sliding. In this case the error does not depend on the method used or on the type of interface: the flow has uniform properties so the distance between the donor and the target point becomes insignificant. The same reasoning is true also for the type of method used to transfer the information across the interface.
From this consideration is evident that this study was useful as a starting point, to check if there was any kind of conservation error, but it can't be used to study the performance of the three methods or the influence of the discretization: tests with more complex flow field must be done.

5. Double Circular Crown

The inner circumference of the internal circular crown has a radius $r_1 = 8$, the circumference at the interface has a radius $r_2 = 10$ and the external one has a radius $r_3 = 12$. The grid is thus divided in two different zones: the internal zone is kept fixed throughout all the simulations while the external is the rotating one. The inner fixed circumference represents the inlet, the external one is the outlet. This results in a radial field, with the flow entering into the domain from the inner circle, crossing the interface and then leaving the domain at the external circumference.
A simulation with only one zone is also performed and it has been taken as a reference. The boundary conditions in this case are the same of the multi zones simulations; the domain has an internal radius r_1, an external r_3 and the grid is kept fixed.
The convective fluxes were computed using the Roe[13] method with Monotonic Upwind Scheme for Conservation Laws (MUSCL)[14] to achieve second order accuracy while for the time integration implicit Euler scheme were used.
The time step used for the unsteady simulation both in this and in the multi-zone case was $\Delta t = 0.003s$ for a total number of 800 time iterations. After an initial transient, a steady state was reached after 350 iterations.

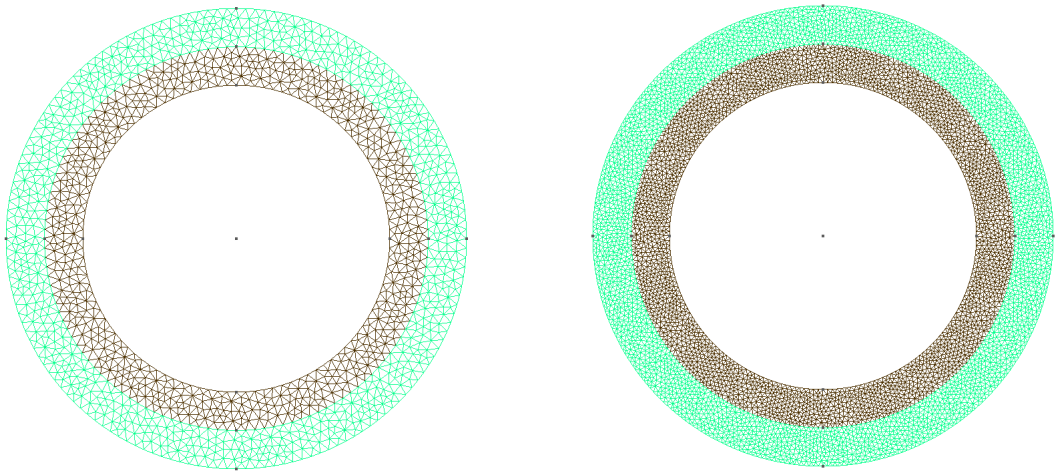

(a) Coarse. (b) Fine.

Figure 2: Double circular crown: Starting grid for the three cases analysed. The mesh on the left is the starting grid for both the coarse and the case with opposite refinement. The second one represent the mesh used in the fine case.

5.1. Coarse grid

The analysis of the sliding mesh algorithms is carried out with the use of two initial meshes and five different types of interface: only the grid on one of the two sides is refined so that the interface becomes more non conformal. The first results shown here are obtained starting from the initial coarse grid shown in Fig. 2a and by refining the external grid. The ratio of the size of the elements between internal and external grid is : $1, \frac{1}{2}, \frac{1}{3}, \frac{1}{5}, \frac{1}{8}$. To conduct the analysis, the mass flux leaving the internal zone is compared with the flux entering the external zone. For a numerical method to be conservative, these two fluxes must be equal, i.e., their difference must be zero. The difference between the flux entering the external zone and the flux exiting the internal zone are displayed in Figs. 3, 4, 5.
As observed, in this scenario, the differences in values are consistently positive across all five types of interfaces. This indicates that the mass flux entering the external zone is larger than the flux exiting the internal zone. If we compare the plots we can notice that in the same size case the three method show almost the same average value and a similar oscillating behaviour. By refining the mesh the error increases; the flux difference for the nearest neighbor approach reaches values that are more than two times bigger than the other two methods. The average values with isoparametric and weighted average approach are pretty similar but the latter shows much larger oscillations. These differences are then averaged and normalized dividing them by the value of the flux that exits from the internal zone. The results of this operation are shown in Table 2:

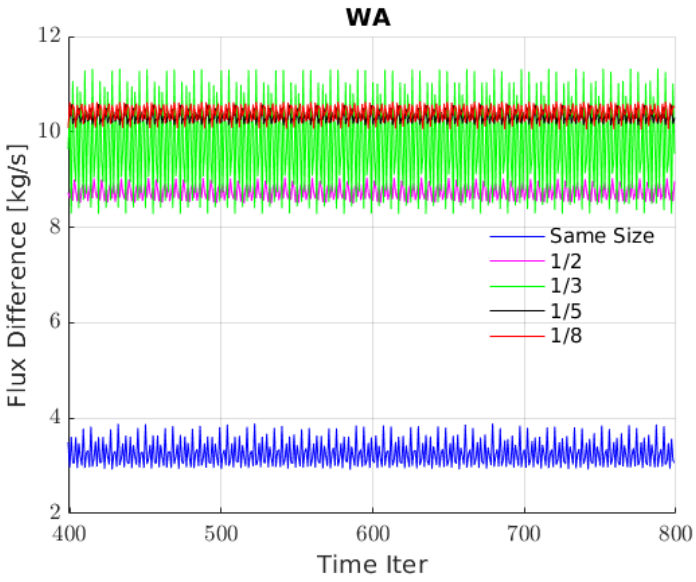

Figure 3: Double circular crown: Difference between entering and exiting mass flux for Weighted Average method with different kind of interfaces.

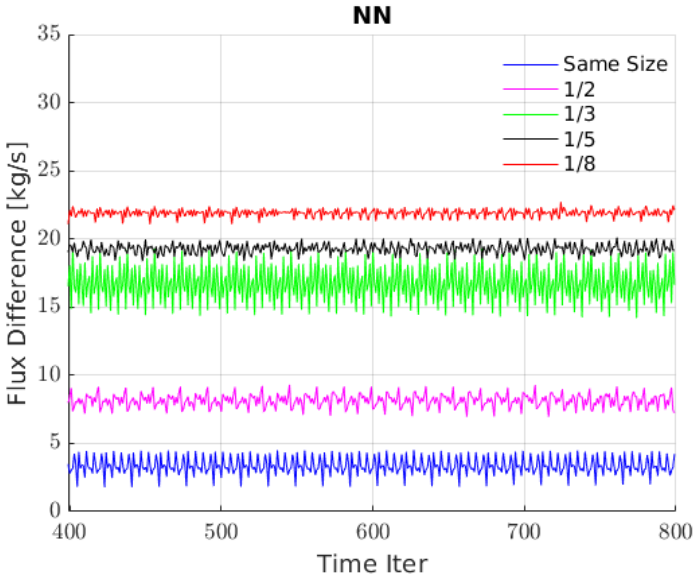

Figure 4: Double circular crown: Difference between entering and exiting mass flux for Nearest Neighbor method with different kind of interfaces.

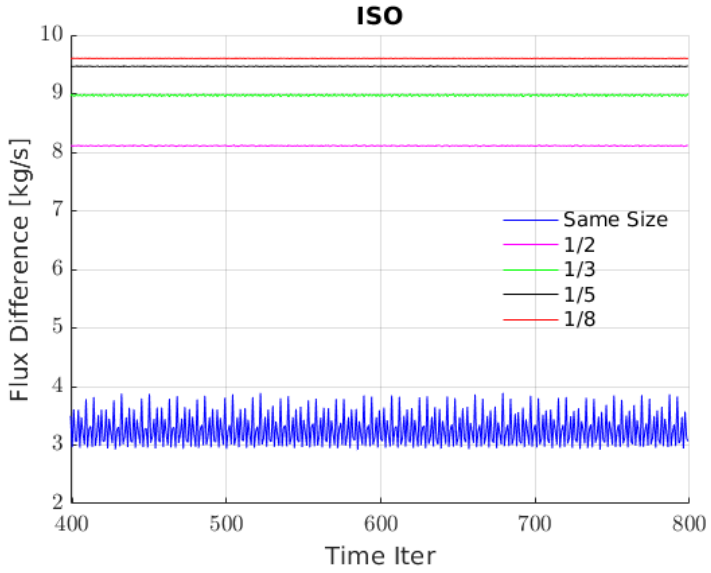

Figure 5: Double circular crown: Difference between entering and exiting mass flux for Isoparametric method with different kind of interfaces.

	WA	NN	ISO
1:1	$3.69E-4$	$3.78E-4$	$3.69E-4$
1:2	$9.91E-4$	$9.20E-4$	$9.16E-4$
1:3	$1.10E-3$	$1.89E-3$	$1.01E-3$
1:5	$1.16E-3$	$2.18E-3$	$1.07E-3$
1:8	$1.18E-3$	$2.47E-3$	$1.08E-3$

Table 2: Double circular crown: Normalized interface mass flux error with coarse starting grid.

5.2. Fine grid

Other simulation have been performed starting with a finer mesh: the edge size of the elements has been halved, Fig. 2b, and than the external zone has been refined as in the previous case. The average value of the normalized difference are displayed in Table 3. As we can see the behaviour is the same: the error grows with the refinement of the external zone and it is larger for the nearest neighbor method. With respect to the coarser simulations, the errors are smaller: in the same size case the difference between the results is almost one order of magnitude. In the scenario involving a $\frac{1}{8}$ interface, the error in the coarse mesh is five times greater when using weighted average and isoparametric methods. Meanwhile, for the nearest neighbor approach, the error is found to be twice as large compared to the fine mesh case. Based on these results we can state that the three methods are not conservative: an error emerges at the interface, and it amplifies with the disparity in the size of grid elements at the interface and, as one should expect, the nearest neighbor simulations exhibit the worst outcomes.

	WA	NN	ISO
1:1	$5.07E-5$	$4.56E-5$	$5.07E-5$
1:2	$2.15E-4$	$2.34E-4$	$1.95E-4$
1:3	$2.47E-4$	$9.09E-4$	$2.22E-4$
1:5	$2.61E-4$	$1.27E-3$	$2.34E-4$
1:8	$2.64E-4$	$1.44E-3$	$2.36E-4$

Table 3: Double circular crown: Normalized interface mass flux error with fine starting grid.

5.3. Opposite discretization

In this paragraph, the outcomes of simulations conducted using the same configuration as the initial case will be examined. The initial grid is once again the coarse one reported in Fig. 2a; the only variation lies in the discretization method: in this scenario, the external zone remains the rotating zone, maintaining its original grid, while the internal zone undergoes refinement to achieve the opposite of the previously discussed five types of interfaces. The average values of the error in the fluxes at the interface are shown in Table 4.

	WA	NN	ISO
1:1	$3.69E-4$	$3.78E-4$	$3.69E-4$
1:2	$-5.74E-4$	$-4.91E-4$	$-4.94E-4$
1:3	$-7.14E-4$	$-6.42E-4$	$-6.11E-4$
1:5	$-8.01E-4$	$-7.30E-4$	$-6.80E-4$
1:8	$-8.29E-4$	$-7.38E-4$	$-6.98E-4$

Table 4: Double circular crown: Normalized interface mass flux error with coarse starting grid and opposite refinement.

The initial observation here is that the first row of the table is identical to the first row in Table 2, and these are the only positive values. Conversely, all the remaining rows exhibit negative values, indicating that, with this particular refinement, the flux leaving the internal zone exceeds the flux entering the external zone. Therefore, we can assert that refining the external zone results in an anomalous generation of mass flux, while refining the internal grid leads to a leakage of mass flux.
Another noteworthy observation in the simulation conducted with this setup is that, despite the errors obtained with this type of refinement being negative, their absolute values are lower than those presented in Section 5.1. Moreover, the disparity in errors among the three methods decreases. Currently, the highest error is observed with the weighted average approach in the context of the $\frac{1}{8}$ interface. The isoparametric method yields the lowest error, while the nearest neighbor method produces an error that falls between the other two. The explanation of this change in the behaviour lies in the different refinement. In all the simulations of the double circular crown, since the direction of the flow goes from the inner zone to the external one, the latter represent the target zone and the former is the donor one. This means that if the refinement is performed only on the inner zone the number of nodes of the donor interface will be greater than the number of nodes on the target side. As a consequence, every target node will have a donor node very close to it. Due to this fact, even though the flow field presents gradients, the error introduced by a theoretically less accurate method, like nearest neighbor, turns out to be smaller than expected. On the other hand, if the refinement is conducted only on the target zone, few target nodes will have a relatively close donor node, while the other target nodes will be more distant from their donor node. This fact has the biggest impact on the nearest neighbor method, and that is the reason why, even though in this case the starting grid is coarser than the mesh in Sec 5.2, the maximum error is smaller than the one obtained with finer mesh and target refinement.

6. Inviscid Vortex Advection

The next case analysed consists in the advection of an isentropic vortex. This is a benchmark commonly employed to assess the accuracy of numerical methods, as it represents an analytical problem governed by the

compressible Euler equations. As described by Yee et al. [15] and in Pezzano, Duvigneau [16] the time evolution of this type of flow is governed by the eqs. 1:

$$\begin{cases} \rho = \left(1 - \dfrac{\gamma - 1}{16\gamma\pi^2}\beta^2 e^{2(1-r^2)}\right)^{\frac{1}{\gamma-1}} & \text{(1a)} \\ u = 1 - \beta\dfrac{y - y_0}{2\pi}e^{1-r^2} & \text{(1b)} \\ v = \beta\dfrac{x - t - x_0}{2\pi}e^{1-r^2} & \text{(1c)} \\ p = \rho^\gamma & \text{(1d)} \end{cases}$$

In these equations the distance from the vortex center is $r = \sqrt{(x - t - x_0)^2 + (y - y_0)^2}$, $x_0 = 5$, $y_0 = 0$ are the initial coordinates of the vortex core and $\beta = 5$ is the vortex intensity. The vortex has a radius $r_v = 0.4$ and a Mach number $M = 0.5$. The computational domain consists in a rectangular box with dimensions $[2.5, 10] \times [-2, 2]$ and periodic boundary conditions are used on all the boundaries. The analysis of the sliding mesh algorithms is carried out by comparing their solutions with the one obtained in a simulation conducted with one single zone. In the case of multiple zones simulations, the inner region is a circular zone with radius $r_1 = 1.5$ and center coincident with the initial position of the core of the vortex. This zone rotates anticlockwise with a velocity of 10 rad/s and fixed time step $\Delta t = 0.004$ s is used. The vortex is then advected downstream, crossing the interface between the two zones. During the advection, the flow structure of the vortex is preserved and an exact solution can be computed. The objective of this study is then to evaluate the effectiveness of sliding mesh algorithms in preserving vortex characteristics as the vortex moves from one side to the other.

6.1. Coarse grid

As previously done in the case of the two circular crowns, the analysis starts from a coarse grid, composed by 28574 triangular elements. The baseline coarse mesh is displayed in Fig. 6. The simulations ran for 2000 time iterations (corresponding to a physical time of 8 s) and the convective fluxes are once again computed using Roe[13] upwind scheme with the use of MUSCL[14] reconstruction to achieve second order accuracy. The grid of the internal rotating zone is then refined, dividing by two and by three the size of the elements of the initial grid.

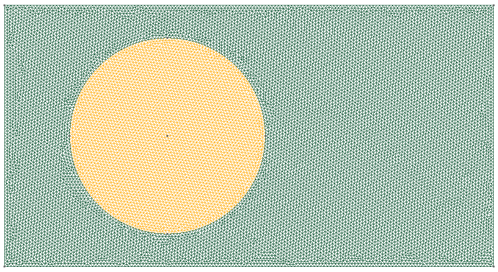

Figure 6: Inviscid vortex test: Starting grid for the two zones simulations.

The study begins with the evaluation of the global conservation error:

$$\varepsilon = \int_\Omega \rho_{t_n+1}\, d\Omega - \int_\Omega \rho_{t_n}\, d\Omega + \int_{t_n}^{t_{n+1}} \oint_{\partial\Omega} \rho \mathbf{u}\, d\Gamma\, dt \tag{2}$$

The time evolution of the error, computed using this formula for grids with elements of equal size, is illustrated in Fig. 7. The first thing to notice is the disparity in errors between the weighted average and nearest neighbor methods: the former is two orders of magnitude smaller than the latter, despite both being relatively small. Actually, their difference becomes evident only during the first half of the simulation, when the vortex crosses the interface. Within this temporal window, the conservation error exhibits positive and negative peaks. As expected, once the transition to the fixed zone is complete, the two errors converge to nearly equal values.

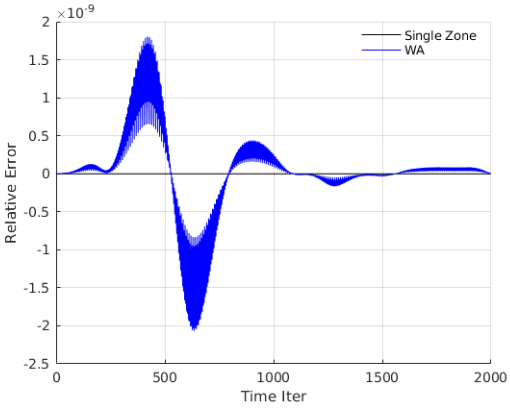

(a) Single Zone VS Weighted Average.

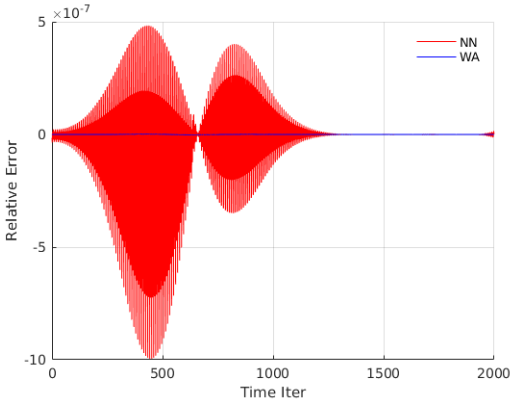

(b) Nearest Neighbor VS Weighted Average.

Figure 7: Inviscid vortex test: Conservation error comparison between single zone simulation and sliding mesh techniques on two grids with elements of the same size. Notice that in the second plot, where the y-axis has values two order of magnitude higher than the first one.

Reducing the size of the elements in the internal grid by half results in errors of the same order of magnitude. However, this time, the computed values exhibit a different behavior, with less pronounced peaks. The variation in shape increases when the internal zone is further refined, in particular with the use of the weighted average method.

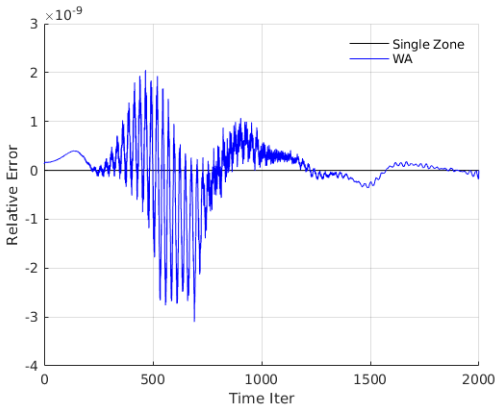

(a) Single Zone VS Weighted Average.

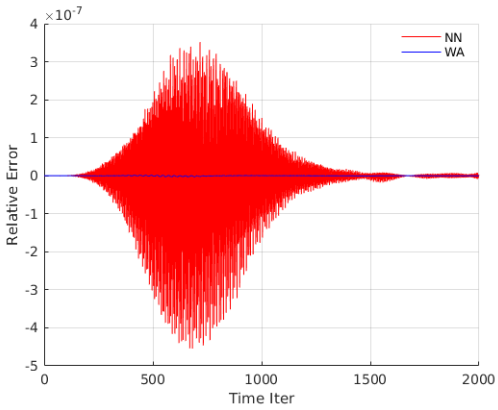

(b) Nearest Neighbor VS Weighted Average.

Figure 8: Inviscid vortex test: Conservation error comparison between single zone simulation and sliding mesh techniques on two grids where the elements of the internal one has half the size of those of the external zone.

As evident from Figures 8 and 9, the error associated with the nearest neighbor approach decreases slightly with refinement. Nevertheless, with the coarse initial mesh, the error for the weighted average method remains smaller. The behaviour of the global conservation errors associated to the isoparametric method is found to be equal to the weighted average one; therefore, its plots are not presented here.
Continuing the analysis, the focus shifts to the flux that crosses the sliding interface. As previously done in the case of the two concentric circles, two mass fluxes have been computed during the simulation: the mass flux through the external interface and the mass flux across the internal interface. The difference between these two fluxes is then normalized by dividing them by the mass flux computed on the internal interface. The trend of these values for the three different interfaces is reported in Fig. 10. As well as the global conservation error, the maximum discrepancies occur when the vortex crosses the interface. Before the onset of the crossing and after that the vortex has completely moved to the external zone, the difference in interface fluxes becomes significantly smaller, and almost no distinctions can be found between weighted average and nearest neighbor approach. Once again, the case of two meshes with the same element size is the one that presents the largest difference between the two methods. Interestingly, this time, refining the internal zone results in a decrease in the error for both methods. Moreover, as observed in the global conservation error, the difference between the

weighted average and nearest neighbor diminishes for finer grids.

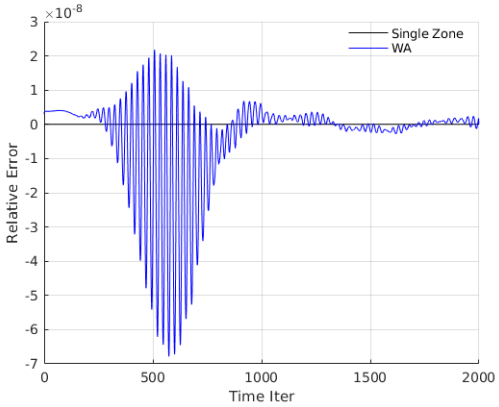

(a) Single Zone VS Weighted Average.

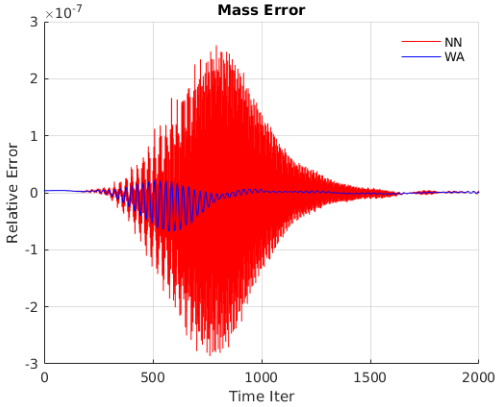

(b) Nearest Neighbor VS Weighted Average.

Figure 9: Inviscid vortex test: Conservation error comparison between single zone simulation and sliding mesh techniques on two grids where elements of the internal one are three times smaller than those of the external zone.

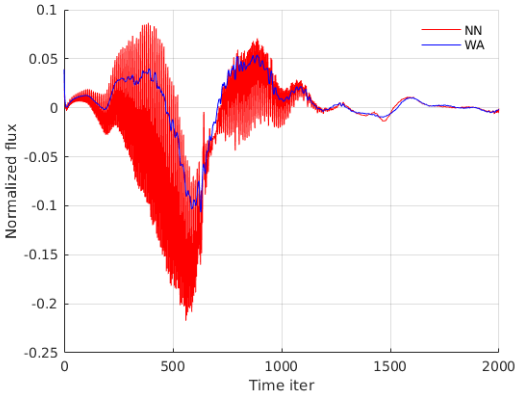

(a) Same size interface.

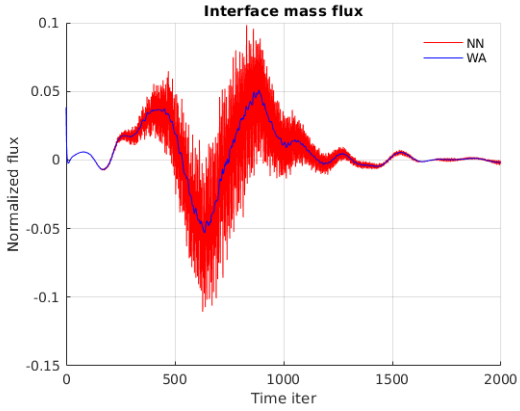

(b) One half interface.

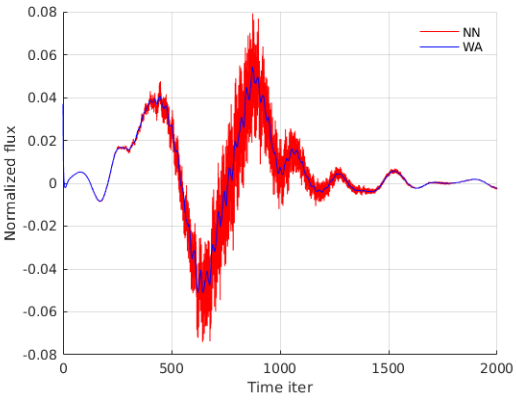

(c) One third interface.

Figure 10: Inviscid vortex test: Difference between mass flux crossing the external and the internal interface for the different kind of grids. The discrepancies between weighted average and nearest neighbor decrease with the refinement of the internal zone.

This is the same trend encountered in the previous test case and the explanation is the same as before: by

refining the internal grid we are refining only the *donor zone*. At the initial time the vortex is placed exactly at the center of the internal zone. Once the simulations are started the internal region rotates while the vortex is advected downstream. Given that the flow moves horizontally from left to right, the vortex will cross the right side of the circumference that defines the inner zone.
This means that, in the crossing spot, the *donor zone* is the one located on the left of the interface, i.e. the internal rotating region. This is the reason why refining the internal grid leads to a reduction in the difference between weighted average and nearest neighbor. As seen in the global conservation error, the interface flux of the isoparametric method closely mirrors the pattern of the weighted average, so it's not reported.
Although the global conservation errors are quite small, the difference in interface fluxes exhibits non-negligible values. The most effective way to evaluate the impact of the loss of conservativity at the interface is to observe how well the vortex properties are preserved after its transition to the fixed zone.
The focus of this analysis will be put on the pressure value at the core of the vortex to examine how much it changes during the simulation. Theoretically this value must be constant during the entire simulation. The values obtained from the multi-zone simulations are compared with those of the simulation performed with one single zone. The plots in Fig. 11 shows the variation of the value of the pressure at the center of the vortex during its motion across the domain. The black line represents the results of the reference simulation. Since, in this initial case, the simulations are conducted with a coarse mesh, a slight amount of numerical diffusion occurs, leading to a small increase in pressure throughout the simulation.

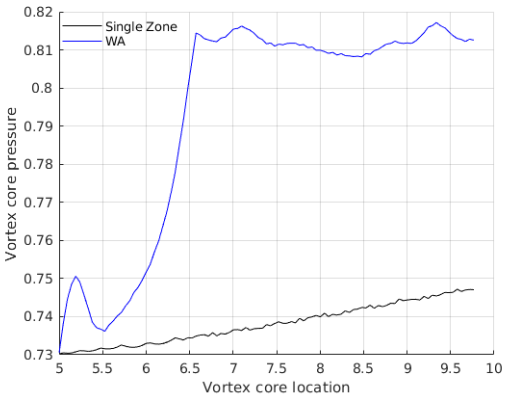

(a) Same size interface.

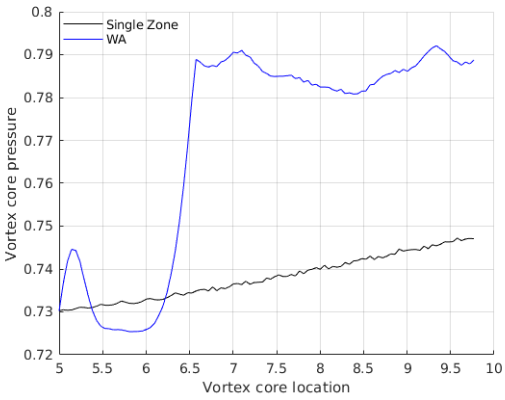

(b) One half interface.

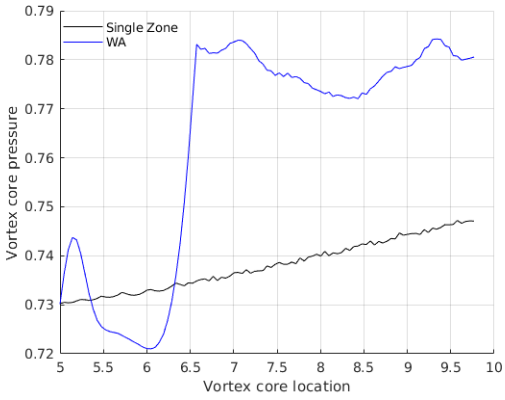

(c) One third interface.

Figure 11: Inviscid vortex test: Evolution of the pressure value at the center of the vortex as it is advected downstream.

The three plots depict the comparison between the reference solution and the results obtained using the weighted average method. They all exhibit a similar behaviour: in the very first time iterations the pressure in the multi-zone simulations grows and then decreases quickly. With the same-size interface, the value never reaches that of the reference; conversely, with half and one-third interfaces, this rapid drop causes the pressure to reach values even lower than the reference. After this drop, when the vortex approaches the interface (which occurs when the core of the vortex surpasses the coordinate $x \approx 6$), there is another increase in pressure. This increase

occurs as the vortex crosses the interface and lasts until the core of the vortex has reached the external zone. The pattern is very similar for the three types of interfaces even though the jump in the pressure decreases a bit with the refinement of the internal zone. Once the vortex has reached the external zone, the pressure trend remains consistent across the three cases. The case with the finest rotating mesh exhibits the lowest pressure values both before and after the vortex transitions from one zone to the other. In contrast, the highest pressure values, indicating the least preservation of vortex properties, are obtained with the coarser internal grid.
In Fig. 12, we illustrate comparisons between the three methods, weighted average, nearest neighbor and isoparametric, highlighting their pressure trends across three different mesh types. Unlike the global conservation error, the disparities between the different approaches are minimal. The lines coincide until the vortex core reaches the interface. Only in the same-size case, the pressure of the nearest neighbor surpasses the values of the other two, while weighted average and isoparametric shows coincident line during the entire simulation. However, once the vortex has moved to the external zone, the three plots become very similar. In the other two cases, no significant differences can be found, with the pressure of the nearest neighbor and isoparametric approach staying slightly lower than weighted average.
Despite these methods exhibiting very similar performance, the errors introduced in the vortex characteristics are quite significant. Changes in the values of vortex properties are present from the beginning to the end of the simulation; the error grows quickly during the transition through the interface, reaching its maximum values right after the cross. The maximum error values are reported in Table 5. As anticipated in the above description, the largest error is associated with the nearest neighbor approach using the coarsest grid. With mesh refinement, the error decreases a bit, reaching values that are almost half of the initial ones. Interestingly, those of the weighted average, which initially were the smallest, become the largest.
Even though the grid of the external zone it's exactly equal to the grid of the single zone simulation, the trend of the pressure at the center of the vortex during its motion in the fixed zone it's quite different from the reference one. Rather than exhibiting an almost linear growth while moving across the domain, in the multi-zone simulation, the pressure shows an oscillating trend.

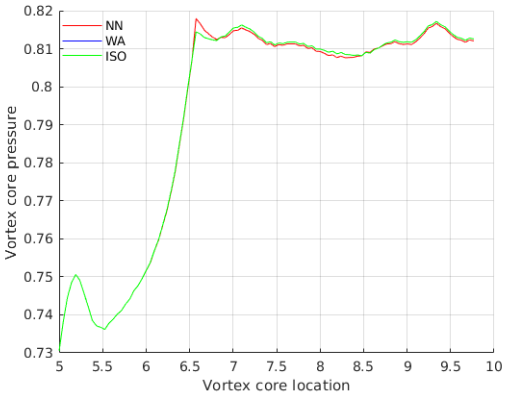

(a) Same size interface.

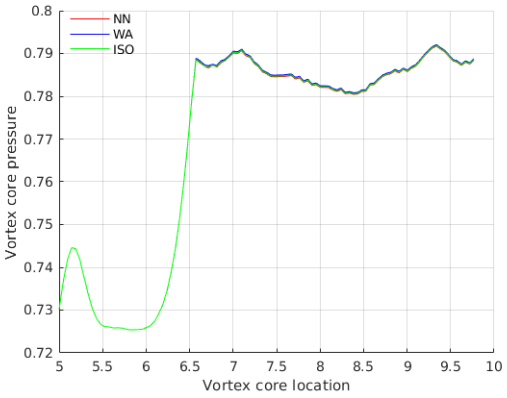

(b) One half interface.

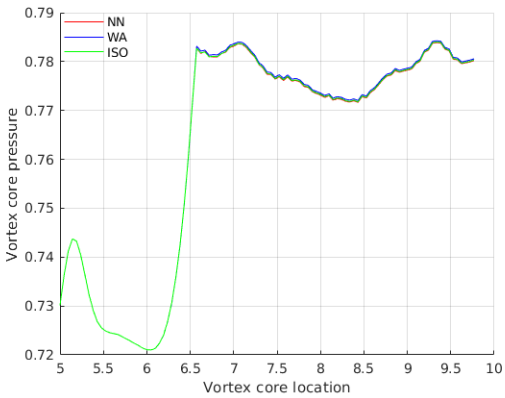

(c) One third interface.

Figure 12: Inviscid vortex test: Comparison of pressure trends using weighted average, nearest neighbor and isoparametric methods across three different mesh types.

	Max Error
1:1	10.85%
1:2	7.42%
1:3	6.57%

(a) Weighted Average.

	Max Error
1:1	11.30%
1:2	7.37%
1:3	6.51%

(b) Nearest Neighbor.

	Max Error
1:1	10.85%
1:2	7.39%
1:3	6.51%

(c) Isoparametric.

Table 5: Inviscid vortex test: Maximum error on the pressure at the core of the vortex.

To better understand the consequences of the sliding interface on the vortex, three new plots are considered: Fig. 13 illustrates the pressure profile along a horizontal line where the core of the vortex is expected to lie. Since the difference in the pressure between the methods are found to be small, here are reported only the results obtained with the weighted average approach.
These plots are taken after 1500 time iterations, and as evident, by this time, the vortex has already completely moved to the external zone. These graphics confirm the results found before, as the biggest difference is found in the same-size case while it becomes less with the grid refinement. Once again we can conclude that the transition through the sliding interface induces a reduction in the vortex intensity.
In addition to this result the value of the pressure far from the vortex is not constant as it should be, but oscillates a bit. Moreover, in these plots seems that the cores of the vortex of the multi-zone simulations are somewhat shifted with respect to the single-zone one.

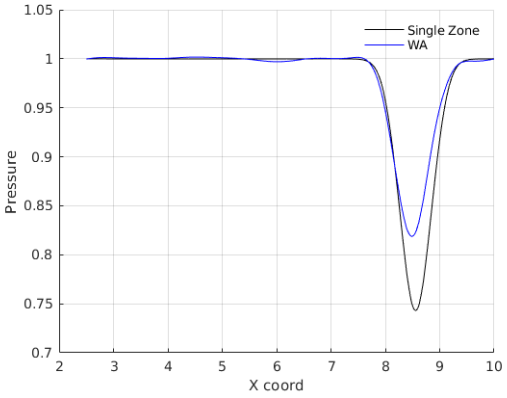

(a) Same size interface.

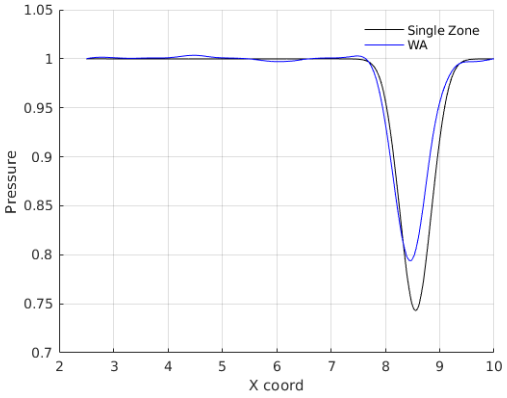

(b) One half interface.

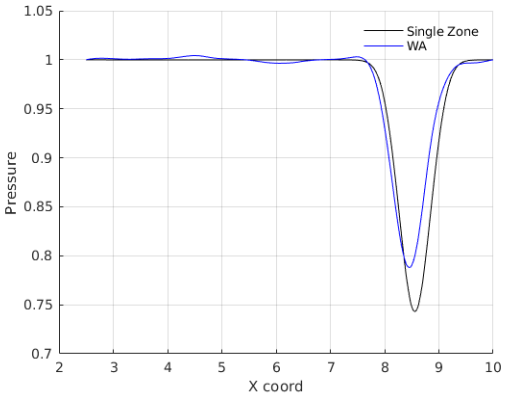

(c) One third interface.

Figure 13: Inviscid vortex test: Pressure profile along a line crossing the entire domain from left to right at a constant $y = 0$. All the three plots shows the comparison between the reference results and the weighted average one. In the three figures can be seen the difference in the values reached by the pressure with the different type of grids.

This is clearly visible in Fig. 14 where the pressure contours of the vortex after 1500 time iterations are reported. In these pictures the black lines represent the contours of the reference solution and the red lines show the isobars

obtained with weighted average method. Here, we can notice that the intensity of the vortex is not the only thing changing through the interface; the contours are no longer circular, and the position of the vortex appears shifted towards the upper left.
The values of the displacement of the vortex in the multi-zone simulations compared to the reference are quantified in table 6. The angular displacement is defined as the angle formed by the line connecting the cores of the two vortex with respect to the positive x-axis. The distance instead is just defined as the length of the segment connecting the two centers.
The obtained results are particularly interesting: in all the three cases the vortex is shifted toward up and left. This might be due to the angular velocity of the internal zone which rotates in a anticlockwise sense. Another thing to notice here is that both the angular displacement and the distance are almost equals in the same and half-size case. With the last refinement instead both the angle and the distance between the vortexes increase. Conversely to the vortex intensity, which exhibits the largest error in the same-size case, the major changes in the shape and position appear in the case with the finer internal grids.

	Angular Displacement	Distance
1:1	126.54°	0.1316
1:2	126.55°	0.1317
1:3	131.76°	0.1793

Table 6: Inviscid vortex test: Vortex displacement from the reference in terms of angle with respect to the horizontal line and distance between the cores of the vortex. These values are obtained after 1500 time iterations.

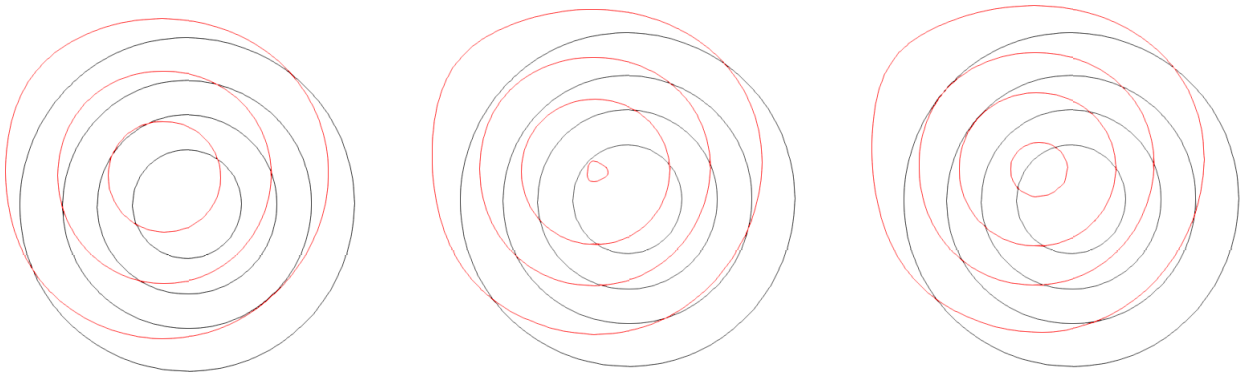

(a) Same size interface. (b) One half interface. (c) One third interface.

Figure 14: Inviscid vortex test: Pressure contours of the vortex after 1500 time steps. The red lines represent the contours of the vortex simulated with the multi-zone grid and weighted average method. The black lines are the pressure contours of the reference solution. The three images show the contours obtained with the three different kind of grids.

6.2. Fine Grid

Additional simulations were conducted by refining the initial grid, halving the size of the elements. A new reference solution was then obtained using a mesh composed of 112,480 triangular elements. Similarly to the coarse case, the preservation of vortex properties was tested by changing the discretization of the internal zone, reducing the dimensions of its elements by 2 and 3. Other than the mesh, the simulation setup remains unchanged: the initial position of the vortex is still at $x_0 = 5$, $y_0 = 0$ with a radius $r = 0.4$ and intensity $\beta = 5$. The analysis of these new results follows the same path as the previous one, beginning with the examination of the global conservation error.
Similar to the coarse simulations, the isoparametric and weighted average methods have produced nearly identical results regarding mass conservation. For this reason, in the following analysis, only the results of the weighted average will be considered.

The error in the same-size case exhibits a couple of differences compared to the coarse case: with the weighted average method, the absolute value of the error has higher peak, while, conversely, with the nearest neighbor method, the error is almost half of its coarse counterpart.

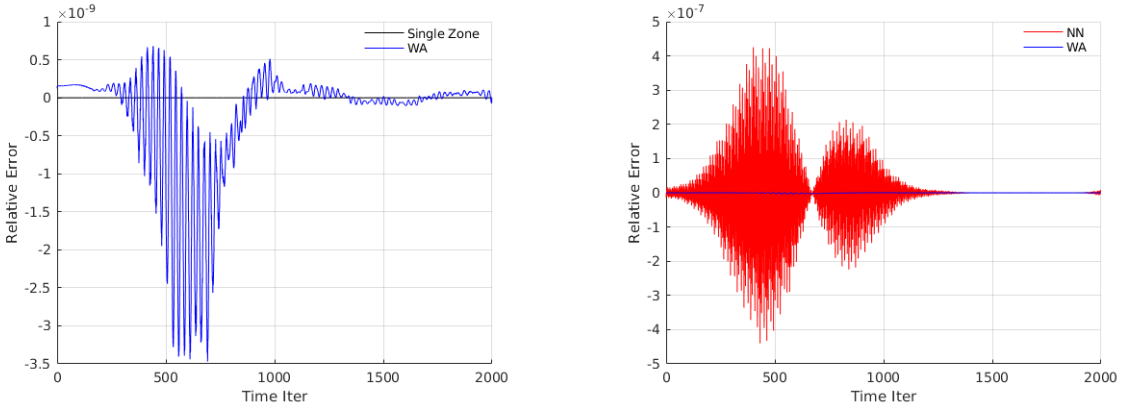

(a) Single Zone VS Weighted Average. (b) Nearest Neighbor VS Weighted Average.

Figure 15: Inviscid vortex test: Conservation error compare between single zone simulation and sliding mesh techniques on two grids with elements of the same size.

With the first refinement of the internal zone, this time the conservation error gets two order of magnitude higher for the weighted average technique. In contrast with the previous test, the errors of the two method are now more similar. Moreover with this finer mesh, the error presents some oscillations even when the vortex has completely gone from the initial zone to the second one.

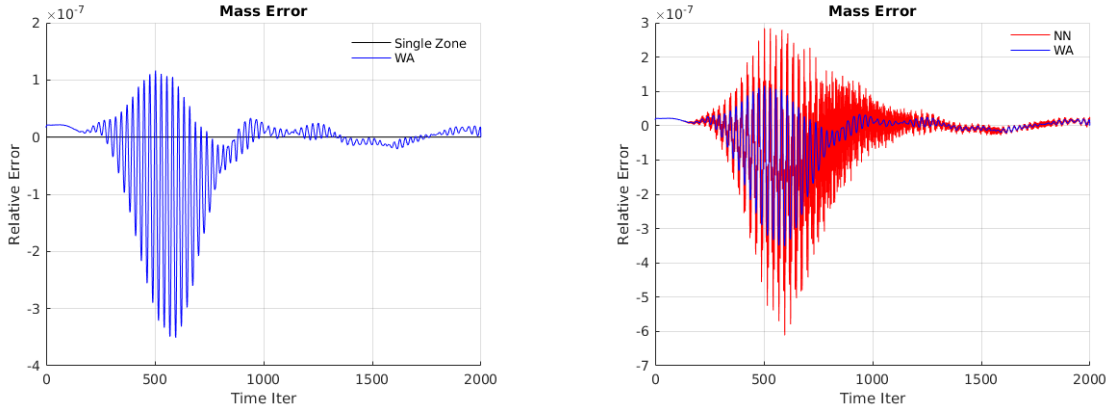

(a) Single Zone VS Weighted Average. (b) Nearest Neighbor VS Weighted Average.

Figure 16: Inviscid vortex test: Conservation error compare between single zone simulation and sliding mesh techniques on two grids where elements of the internal one has half the size of those of the external zone.

This is more evident in Fig. 17: with this setup, the order of magnitude of the errors of both methods is increased by one, and the peak in the error is no longer as pronounced. In the coarse case, the peaks that occurred during the transition across the interface were even one thousand times larger than the values of the last iterations. With this finer mesh, instead, the oscillations have almost the same order of magnitude during the entire simulation and no significant difference can be found between the three methods used.
These are trends that can be observed also in the study of the mass flux at the interface. As depicted in Fig. 18, the error associated with the weighted average method increases with the refinement of the internal grid. On the other hand, the error for the nearest neighbor method decreases with the first refinement and then increases with the second one. About the first two kind of interface there are no other comments to report, the behaviour of the interface flux with this finer grid mirrors the coarse one.
In the case with element size ratio at the interface equal to 1/3 instead, two observations have to be made: the first one is that the difference between the two proposed techniques becomes almost null. The second

observation pertains to the behavior of the interface flux after the vortex transitions into the fixed zone: as illustrated in Fig. 19, there are oscillations approximately three times smaller than the peak values, even when the vortex is moving only in the external zone.

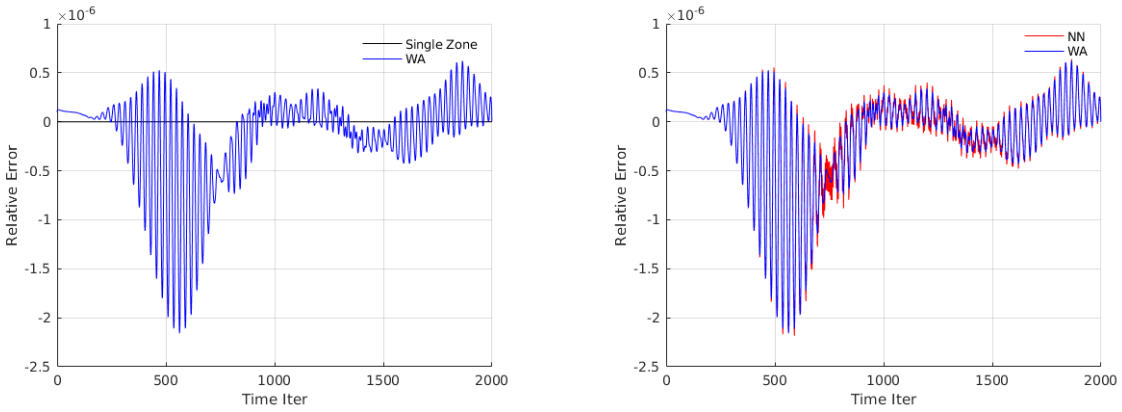

(a) Single Zone VS Weighted Average. (b) Nearest Neighbor VS Weighted Average.

Figure 17: Inviscid vortex test: Conservation error compare between single zone simulation and sliding mesh techniques on two grids where elements of the internal one are three times smaller than those of the external zone.

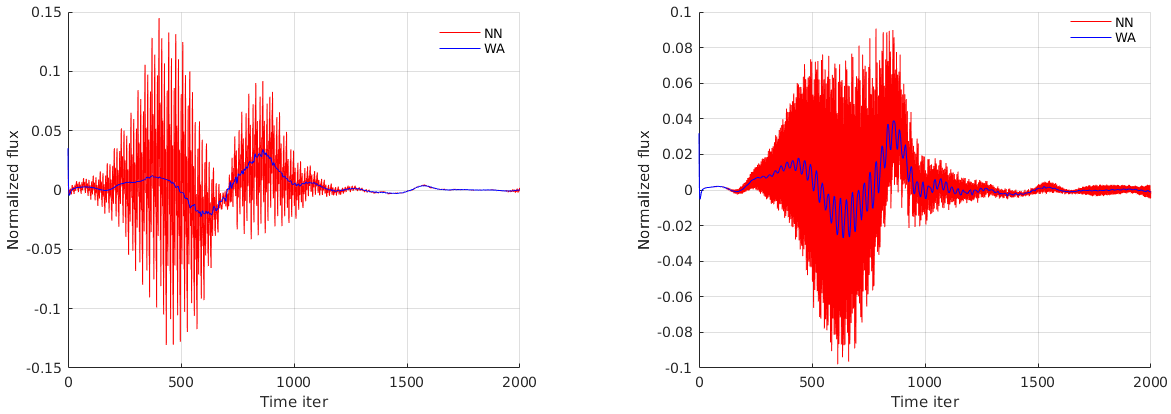

(a) Same size interface. (b) One half interface.

Figure 18: Inviscid vortex test: Error between mass flux crossing the external and the internal interface in the case with same-size and half-size grids. It must be noted that with the one half interface the the absolute value of the differences becomes lower.

So far we have seen that both the conservation of mass in the computational domain and the flux difference at the interface exhibit different behaviour if the entire grid is refined. As shown in the next paragraph, instead, the trend in the value of the pressure at the core of the vortex presents some similarities to the coarse case.
Before starting the comparison, it is important to notice that by the use of a much finer grid, the properties of the vortex are slightly better preserved in the reference simulation. Indeed, the disparity between the pressure values at the beginning and the end of the single-zone simulation is nearly negligible.
As previously observed in Sec. 6.1, here too, as shown in Fig. 20, the core pressure undergoes a rapid and brief increase in the initial iterations, followed by an equally sharp descent. These decreases cause the pressure to reach values lower than the reference, and these minima are highly dependent on the grid discretization. Within the same-size framework the minimum is reached once the core of the vortex is located at $x = 5.5$, then it stays almost constant until the external part of the vortex approaches the interface. At this point there's the second growth already seen also in the coarse case.
In the other two scenarios instead, the pressure keeps dropping until the vortex reaches the interface. Unlike the same-size grid, where the increase begins when the external portion of the vortex crosses the interface, in

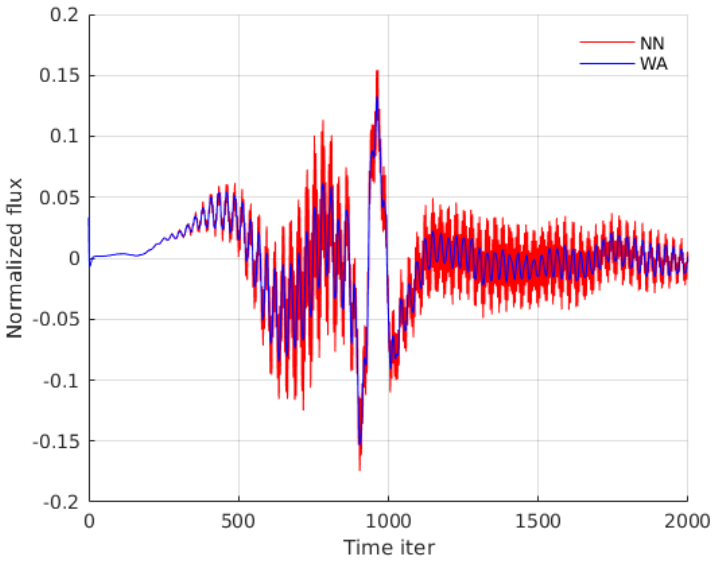

Figure 19: Inviscid vortex test: Mass flux difference at the interface when the internal zone has three times smaller element size. The discrepancies between weighted average and nearest neighbor are very small with this setup.

both half-size and one-third cases, the growth occurs only when the central portion of the vortex reaches the interface.
Once again, after the transition into the external zone is finished, the multi-zone simulations show different trend with respect to the reference one. All three cases exhibit oscillations, whose amplitude seems to depend on the internal grid discretization, despite the fact that the external zone is exactly the same for all three cases.

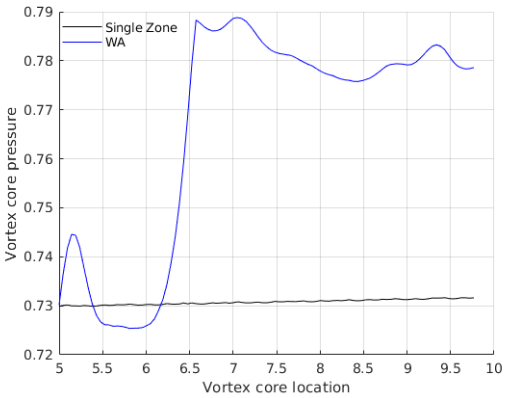

(a) Same size interface.

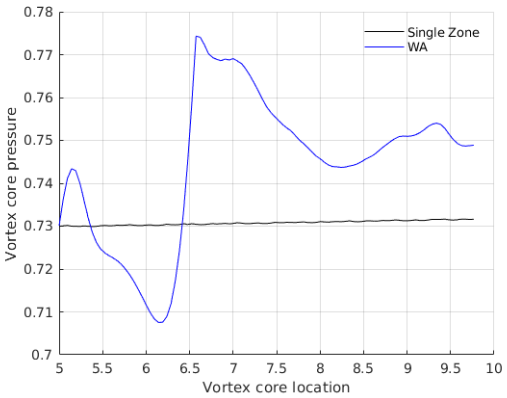

(b) One half interface.

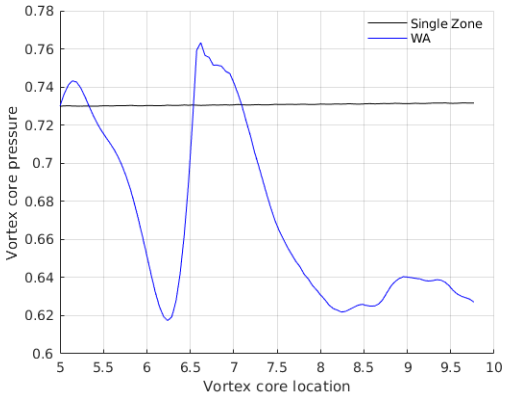

(c) One third interface.

Figure 20: Inviscid vortex test: Evolution of the pressure value at the center of the vortex as it is advected downstream.

This is particularly evident in Fig.20c, where after the transition, the pressure undergoes another sharp drop, resulting in values much lower than the original one. Actually, the pressure drop in the stationary zone is present in all the three cases but it manifests in different manners.
The decline in pressure exhibits nearly identical duration across all three distinct meshes; indeed, it concludes when the vortex reaches the region between $x = 8$ and $x = 8.5$. The intensity of the drop instead, highly depend on the internal grid size. In the same-size case it is very small; it gets bigger with the first internal refinement and then increases again with the second one.
As we will see also later on in the analysis, this type of grid introduces several errors on the vortex characteristics. So far, what emerges from these simulations is that the presence of the sliding interface influences the entire flow field. The behavior of the vortex core pressure doesn't match the reference, neither in the rotating zone nor in the fixed one.
Despite the significant difference from the reference, the discrepancies between the results obtained with the three different methods tested here are minimal. The values of the pressure in the center of the vortex throughout the simulations are almost equals for all the three approaches. As an example in Fig.21 the trends obtained with the three different approaches are reported for the same-size grids.
The maximum errors in the pressure values for the three techniques is displayed in Table 7.

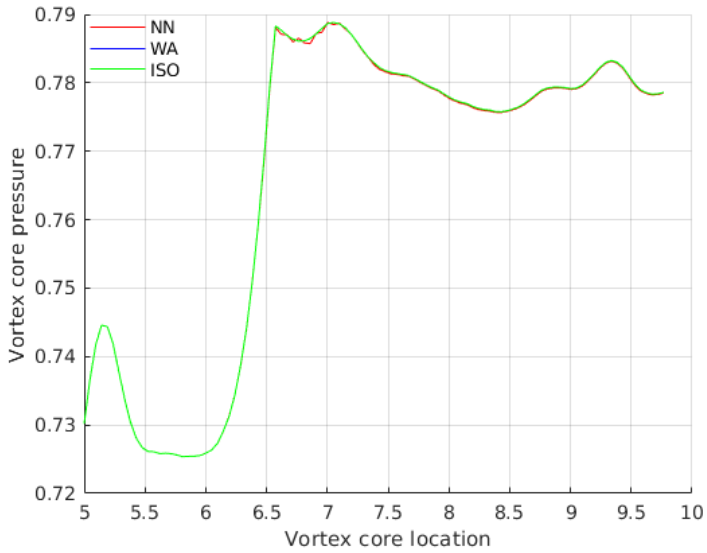

Figure 21: Inviscid vortex test: Comparison between the values of the pressure at the core of the vortex obtained with the three different approaches. As an example in this figure only the same-size scenario is reported. As clearly visible the differences between the methods are minimal.

	Max Error
1:1	7.40%
1:2	6.01%
1:3	15.48%

(a) Weighted Average.

	Max Error
1:1	7.96%
1:2	6.00%
1:3	15.48%

(b) Nearest Neighbor.

	Max Error
1:1	7.94%
1:2	6.01%
1:3	15.48%

(c) Isoparametric.

Table 7: Inviscid vortex test: Maximum error on the pressure at the core of the vortex.

As one should expect from the previous plots, the maximum errors on the values of the core pressure are associated to the one-third interface. As in the previous case the error decreases with the first refinement and the difference between the three methods almost disappear. In the case of a one-third interface instead the error gets two times higher with respect to the initial one independently from the algorithm adopted.
Another confirm of this trend is provided by the pressure profile along a horizontal line crossing the domain at its half. The values of the pressure for these plots are taken after 1500 time iterations, when the vortex has completely gone from the first zone to the second one.

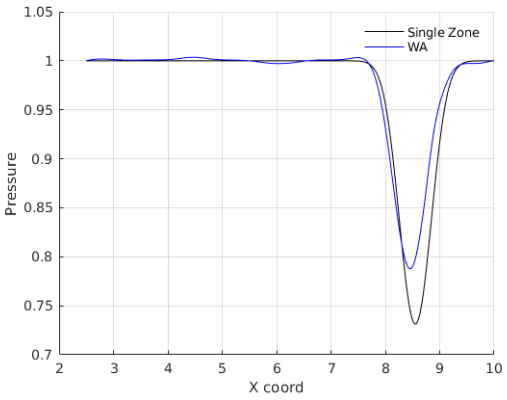

(a) Same size interface.

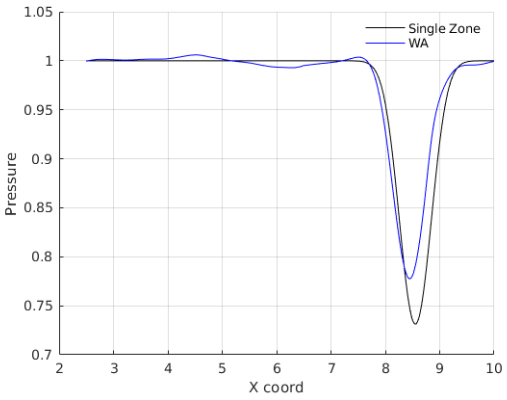

(b) One half interface.

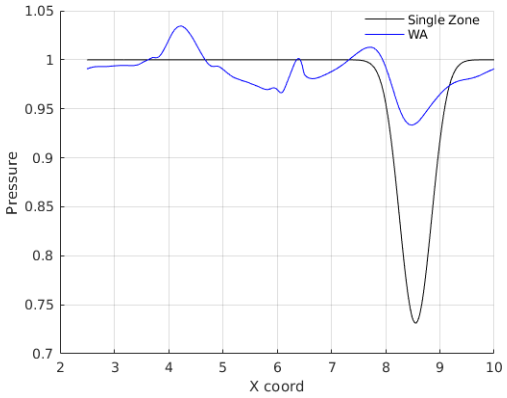

(c) One third interface.

Figure 22: Inviscid vortex test: Pressure profile along a line crossing the entire domain from left to right at a constant $y = 0$ for different types of meshes. In the first two figures can be noticed the difference in the magnitude of the vortex and in its position. Particular attention instead is needed with the third images. The line crosses the domain at a constant $y = 0$ but, with the one third interface the vortex position is shifted toward up and left, so the line just barely touch the external portion of the vortex.

Fig. 22c shows how big is the impact of the one third interface on conservation of the vortex characteristics. While in the cases of same and half-size interface the line along which the pressure is plotted still crosses the vortex near its center, in the one-third case it barely touches its external portion. So the values of the pressure in the plots are that high not because the vortex intensity has changed so much but because the vortex turns out to be shifted.
The effects of the interfaces on the vortex shape and position can be better seen by looking at the compare of the pressure contours of the vortex between the reference solution and the sliding mesh simulations. In Fig. 23 the black lines represent the reference vortex while the red lines represent the results of the weighted average method. As in the previous plots, the pressure contours are computed after 1500 time iterations.
The first thing to be noticed is the shape change: the isobars shows an elongated aspect instead of a circular one. Particularly interesting is to notice the fact that the error on the vortex magnitude in the one half case was lower than the same size one; comparing Fig. 23a and Fig. 23b it's evident that instead the same size interface is the one that leads to less changes in the vortex shape. Coherently to the errors in the vortex intensity, the one third interface is the one with the largest changes in shape. Not only, this case is also the one who shows the largest shifts in the vortex position.
The displacement in the vortex positions is then evaluated by comparing the positions of the points where the pressure is at its minimum, i.e. the cores of the vortexes.

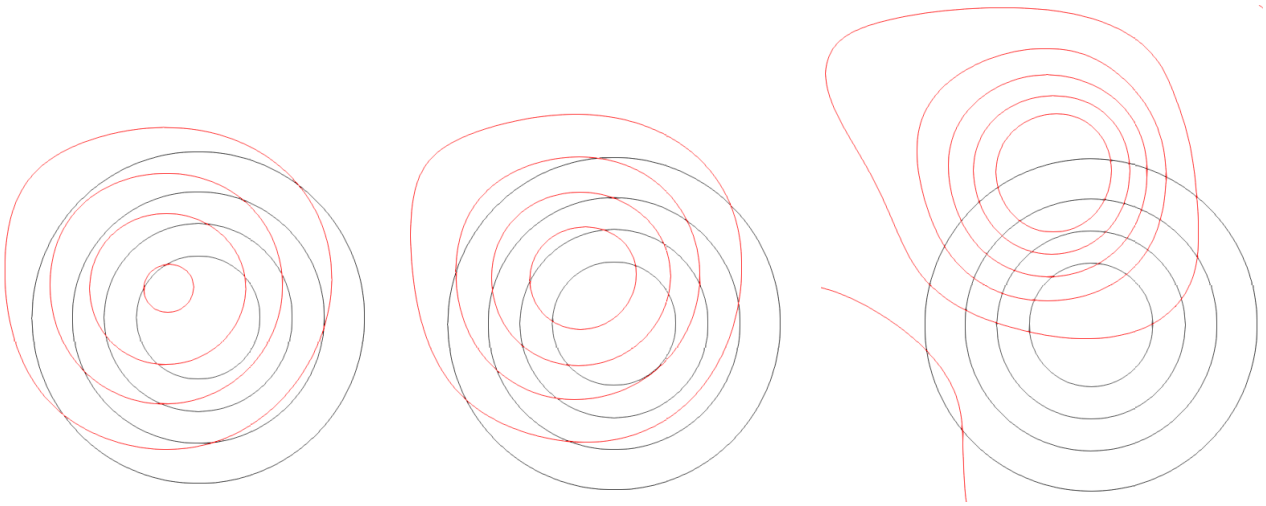

(a) Same size interface. (b) One half interface. (c) One third interface.

Figure 23: Inviscid vortex test: Pressure contours of the vortex after 1500 time steps with fine mesh. The red lines represent the contours of the vortex simulated with the multi-zone grid and weighted average method. The black lines are the pressure contours of the reference solution. The three images shows the contours obtained with the three different kind of grids.

The shift in the vortex location is evaluated by means of its angular displacement and its distance from the reference one. The results are shown in table 8:

	Angular Displacement	Distance
1:1	136.02°	0.1389
1:2	123.20°	0.1746
1:3	104.98°	0.5040

Table 8: Inviscid vortex test: Vortex displacement from the reference in terms of angle with respect to the horizontal line and distance between the cores of the vortex.

The angular displacement is again computed with respect to the positive x-axis and the distance is just the Euclidean distance between the two cores.
Two major trends can be observed: the first one is that the angular displacement this time decreases with mesh refinement. The vortex of the same-size is displaced more to the left than upward, while the vortex in the one-third case is almost aligned vertically with respect to the reference one.
If the angle decreases with the refinement, on the contrary, the distance between the centers increases. The first two cases display a similar distance with respect to the single zone one. The radius of the original vortex was $r = 0.4$ so, despite the displacement, they both still share some portions with the reference vortex.
The distance in the case of a one third interface instead is higher than the original radius. This data confirms what has been shown in the previous plot: a horizontal line at $y = 0$ just barely touches the external portion of the advected vortex.
With this kind of interface the properties of the vortex are badly conserved and the changes to the vortex characteristics affect the whole domain: the flow field outside of the vortex presents oscillation in the entire domain instead of being just uniform.
These effects can be seen in Fig. 24 where a flow visualization of the vortex with the four different grid is presented. The color scheme used to represent the pressure is the same in all the four pictures. The images are taken at the same time instant but the position at which they are taken is different: as already seen, in the multi-zone case the vortex position changes with respect to the reference one so each of these figures is centered on its own vortex.
From this images is clearly evident the difference in the vortex magnitude and shape: in the same size interface the lowest values of the color scheme are never reached. The same thing is valid also for the one half case, because the visualizations are taken after 1500 time iterations and at that time the pressure with this mesh is higher than the reference.

The last picture instead shows that this pressure value, i.e. the minimum value reached in the reference, appears not only in one point but in an entire region.
The last thing to notice is the pressure outside of the vortex: in the reference case out of the vortex the pressure reaches the undisturbed value of 1 in all the directions. In all the three multi-zone simulations instead in the top left and bottom right corners the values reached by the pressure are lower. Again, the largest influence on the flow field outside of the vortex belongs to the one-third case.

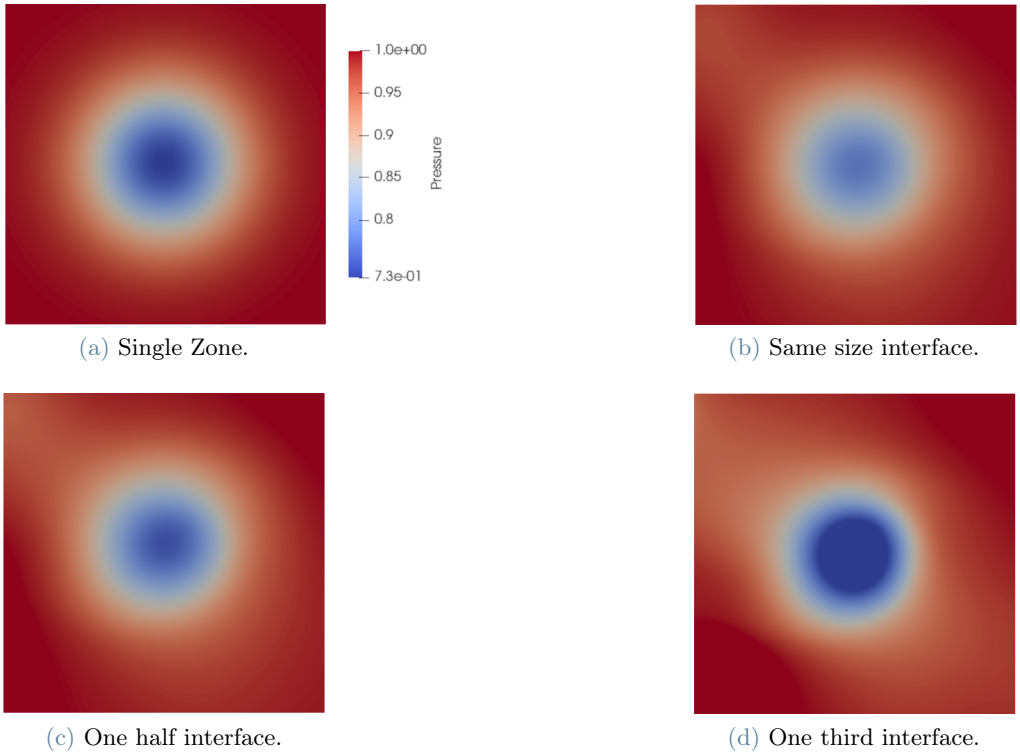

(a) Single Zone.

(b) Same size interface.

(c) One half interface.

(d) One third interface.

Figure 24: Inviscid vortex test: Pressure in the whole vortex after 1500 iterations. The four flow visualizations show the changes in the shape and in the intensity of the vortex in the multi-zone simulations compared to the single-zone result. The first picture shows also the color scheme used in all the four images.

Upon closely examining the results obtained so far, a question arises spontaneously: what could be the reason behind the worsening in the results with the last refinement. The setup of the simulations has been the same for every case, so the only difference can be caused by the grid but, theoretically, a finer grid should preserve better the vortex properties. The answer to this question could lie in the combination of: grid discretization, grid motion and unsteady time step.
So far the time step used has always been the same, $\Delta t = 0.004s$ and the internal zone is rotated with an angular speed of $10rad/s$. This implies that the angular displacement per time step is : $\delta\alpha \approx 2.29°$. Being the radius of the internal zone $r = 1.5$ the tangential displacement of a node of the internal grid during every time iteration is $\delta x \approx 0.06$.
The edge size of an element of the mesh in the fine case is $h = 0.025$. So this means that in the same-size case the relative displacement of the nodes at the interface is equivalent to almost 2.5 element's edge size; in the other two scenarios this value is doubled and tripled.
To investigate if the amount of the relative displacement between the two adjacent grids has an influence on the sliding mesh techniques further simulations have been conducted using the very same setup as before and changing only the value of the time step. The new simulations ran for 20000 time iterations instead of the previous 2000 with a time step 10 times lower, namely $\Delta t = 0.0004s$.
In contrast with the previous approach, since almost no difference were found between nearest neighbor, isoparametric and weighted average here only the results using the latter technique are reported.
As already done so far, the first step of this new analysis consists in the computation of the error on the conservation of mass in the domain for the three different types oh meshes. The results obtained in this scenario are reported in Fig.25.

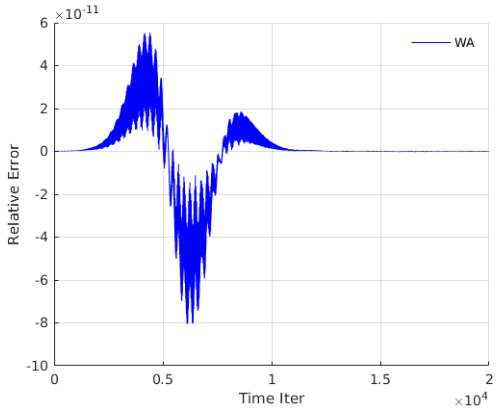

(a) Same size interface.

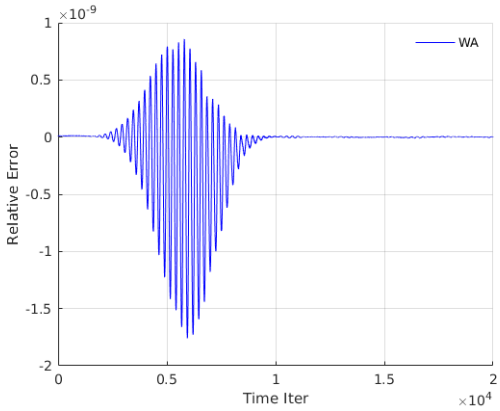

(b) One half interface.

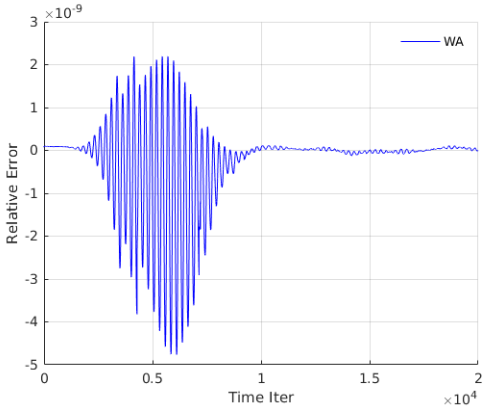

(c) One third interface.

Figure 25: Inviscid vortex test: Mass conservation errors retrieved with fine mesh and smaller time step. The multi-zone simulations of this kind of test are conducted using weighted average approach.

The error in this scenario closely resembles the shape observed in the coarse case. The main differences are that, in the same size case, the error with this time step it's two order of magnitude lower than its coarse counterpart; in the one third case instead the disparities amount to one order of magnitude.
With respect to the error obtained with the finer mesh instead the differences are much bigger: 2 orders of magnitude in the first two cases and 3 in the last one. Furthermore, the errors exhibit peaks during the vortex's transition through the interface, after which they stabilize at values close to machine precision.
The preservation of the vortex properties is once again tested by the study of the evolution of the pressure in the vortex while it moves through the domain. The plots in Fig. 26 shows the trend obtained with the three types of interfaces.
Independently from the mesh or the time step, in the very beginning of the simulation the vortex in the rotating zone experience a rapid growth. This increase is immediately followed by an equal decrease: in the same-size scenario the multi-zone pressure reaches the reference one and then, they keep very close to each other until the vortex arrives at the interface. At that point there's a small increase. The gap in this case is still small compared to the one obtained with a larger time step: in fact the maximum difference between the reference solution and the same-size case amounts to 0.22%.
In the one-half scenario instead the drop leads the pressure toward values lower than the reference. In this case too there's another increase during the interface transition but this time the pressure stays lower. The maximum error with this setup is found to be 0.17%.
The finest grid test follows a trend similar to the one just described, with the only difference that the maximum error amounts to 0.23%.
In addition to the decrease in the relative error on the core pressure there's another difference to notice: with this lower time step, in the external zone, the core pressure in the multi-zone simulations exhibits an increase similar to the single-zone one.

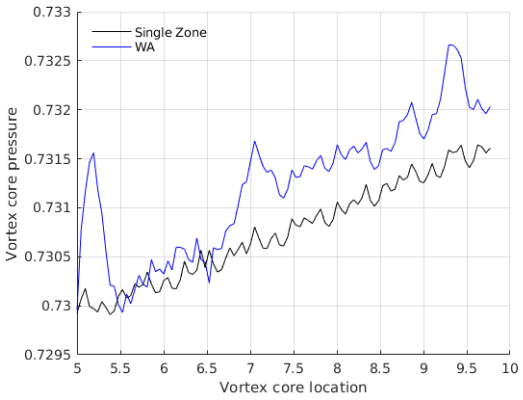

(a) Same size interface.

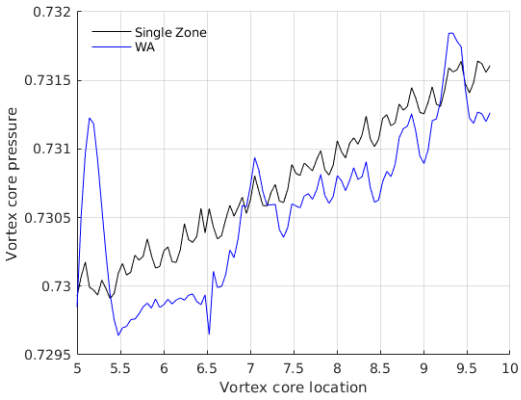

(b) One half interface.

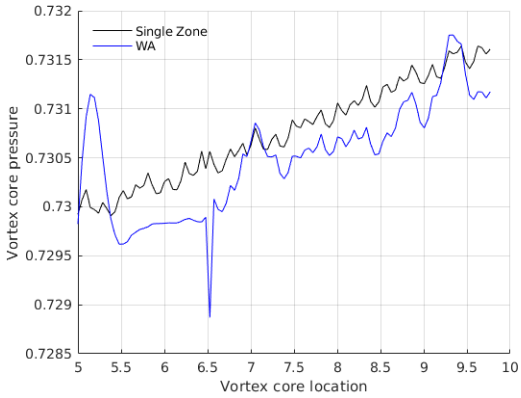

(c) One third interface.

Figure 26: Inviscid vortex test: Evolution of the pressure value at the center of the vortex as it is advected downstream.

For the sake of completeness in Fig. 27 is shown the pressure profile plotted along an horizontal line crossing the vortex at its center.
The plot is done at the same physical time both for the single zone and the multi zone simulations.
The figure reports only the results of the same-size case because all the three multi zone simulations retrieved very similar plots. In contrast to the previous pressure profile, the two lines now coincide from start to finish; no difference in vortex intensity or pressure oscillation far from the vortex can be observed.
Since it is evident from these data, with this small time step, both the shape and the position of the vortex are correctly preserved, and thus, no pressure contour or flow visualizations are needed.

7. Oblique shock

The final case analysed involves a supersonic flow at $M = 2.5$ moving from left to right, encountering a wedge and thereby forming an oblique shock. The main idea of this test is to see how these sliding mesh techniques can deal with sharp discontinuities like a shock wave.
The domain has a total horizontal length of $x = 1.5$ and a vertical one of $y = 1$. The wedge is in the bottom boundary, starting at $x_{wi} = 0.5$, $y_{wi} = 0$ and reaching the right extreme at $x_{wf} = 1.5$, $y_{wf} = 0.2$; the angle created is then $\theta = 11.3°$. As described by Thompson [17], using the relation 3 it is possible to determine analytically the deflection angle β of the flow:

$$\tan(\theta) = \frac{2\cot(\beta)M_1^2\sin^2(\beta) - 1}{(\gamma+1)M_1^2 - 2M_1^2\sin^2(\beta) - 1} \tag{3}$$

The value retrieved in this case is $\beta = 33.12°$ and it can be used to compute analytically the values of the jumps in the flow properties across the shock wave.
As in the previous tests the analysis is carried out by comparing the multi-zone simulations with a single-zone one. Before running all the simulations needed to complete the analysis, a grid convergence study is carried

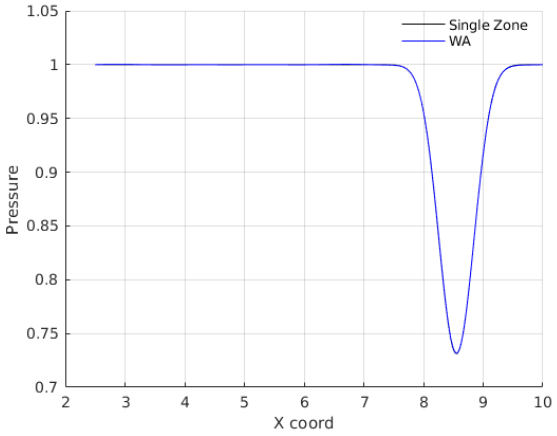

Figure 27: Inviscid vortex test: Pressure profile after 15000 time iterations, plotted along a line crossing the domain at a fixed $y = 0$. The plot in this figure represents the comparison between the same-size weighted average values and the refrence one.

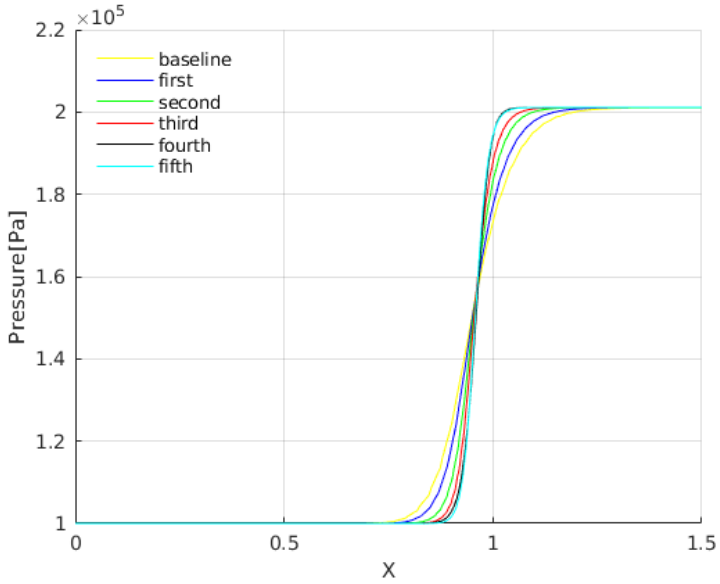

Figure 28: Oblique shock: Grid convergence analysis performed by comparing the pressure profile across the oblique shock.

out. The baseline mesh was a very coarse grid composed by 4268 triangular elements; then it has been refined five times, leading to a finest grid made up by 129714 triangles.
The Fig. 28 shows the results of the grid convergence analysis. Since the values of the pressure after the fourth and the fifth refinement are almost coincident, the fourth grid, consisting in 66629 triangles, has been chosen for the study of the sliding mesh algorithms performances. The internal grid used for the multi-zone simulations is a small circle with radius $r = 0.1$ and centre located at $x = 1$ and $y = 0.3$ as shown in Fig. 29.
After an initial transient, the oblique shock is formed and it crosses the internal rotating zone.
In these simulations the convective fluxes are computed using Harten-Lax-van Leer Contact (HLLC)[18] method and implicit Euler has been employed for the time discretization. The internal zone of the multi-grid computations is rotated at an angular speed of $100 rad/s$ and the time step used for the unsteady simulations is $\Delta t = 1e - 5$.
The first interesting results of this case are displayed in Fig.30.

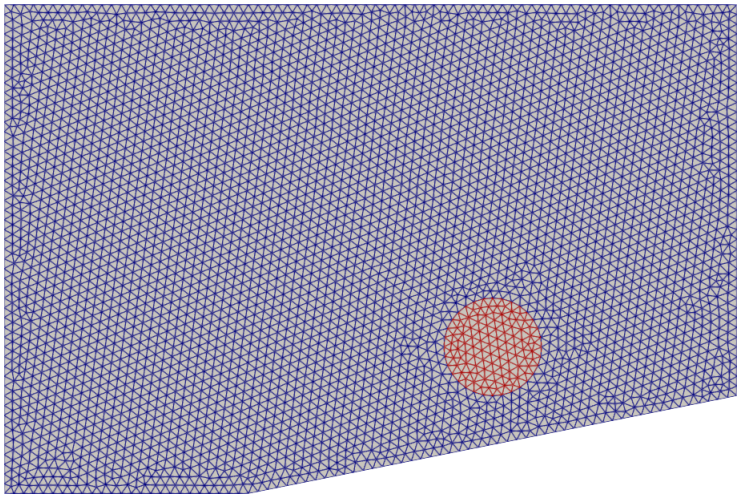

Figure 29: Oblique shock: Example of the mesh with the two zones. In this figure can be seen where the internal zone is placed with respect to the wedge. This is the baseline mesh used in the grid convergence study.

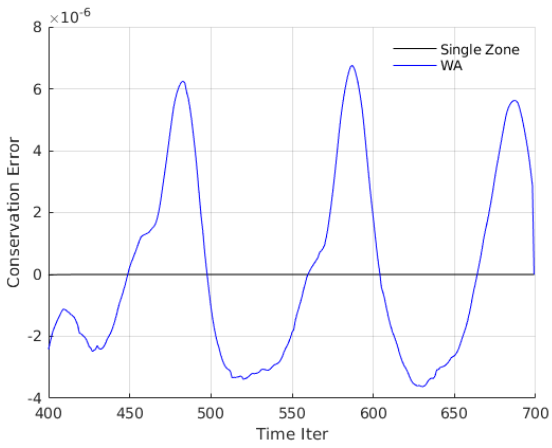

(a) Single zone vs Weighted average

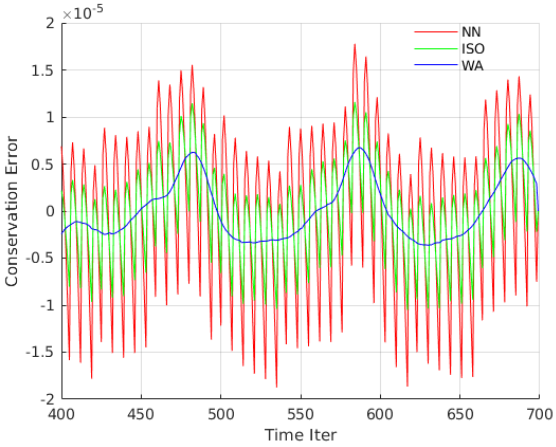

(b) Compare between sliding mesh algorithms

Figure 30: Oblique shock: Mass conservation error once the simulation has reached a steady state. The first pictures show that in multi-zone simulations there's an oscillatory conservation error. The second one shows the comparison between the amplitude and the frequency of the oscillations introduced by the three sliding mesh techniques.

The two plots show the mass conservation error during the last 300 iterations of the simulations. The transient period, during which the shock is developed, in the single-zone scenario, concludes entirely after approximately 450 iterations. From this point onward, the mass and the total energy in the domain remain constant for the rest of the simulation. Since the mass and the total energy show the same behaviour both in the single-zone and in the multi-zone scenarios, only the plots associated to the mass error are shown here.
In the case of multi-zone simulations, the global mass, instead of stabilizing at a constant value, continues to oscillate after each time iteration. The error in mass conservation obtained through the weighted average method exhibits oscillations with an amplitude of the order of 10^{-6}. In contrast to the results obtained for the vortex case, the error associated with the isoparametric method deviates from the pattern observed with the weighted average method reaching larger values. Furthermore, the frequency of the oscillations is considerably higher. In this context, the nearest neighbor follows a similar trend to the isoparametric one, but the amplitude of its oscillations is slightly larger.

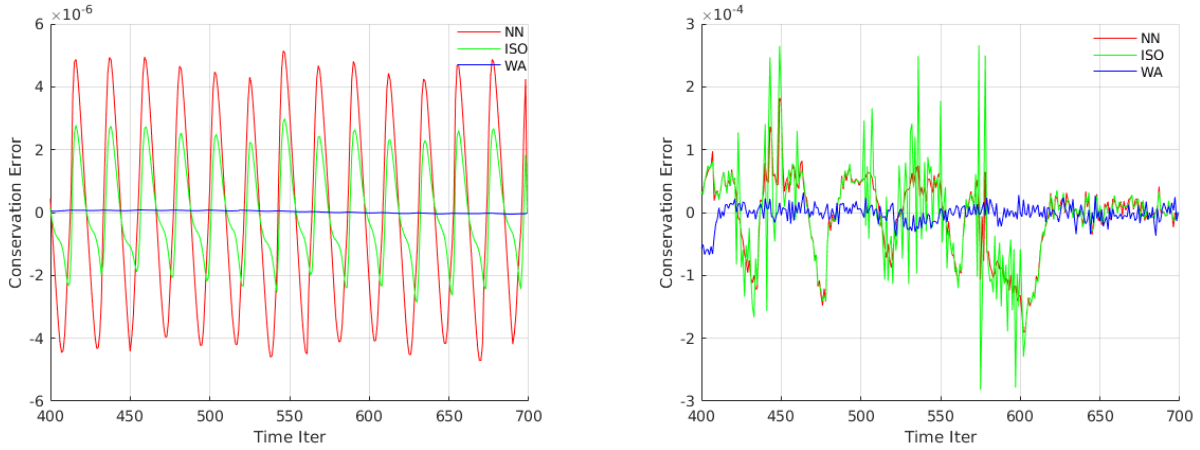

(a) One half interface

(b) One third interface

Figure 31: Oblique shock: The first plot shows the error in the conservation of mass of the three sliding mesh approach with a element size difference at the interface equal to 1/2. The second one shows the error retrieved in case of 1/3 interface. It's important to note that in the second plot the y-axis is two order of magnitude larger than the first one.

The conservation error is subsequently calculated by conducting additional simulations, as shown in Fig. 31, where the grid of the internal zone is refined to attain two interface ratios: 1/2 and 1/3.
After the initial refinement, all three methods have undergone an improvement in terms of conservation errors. In particular, the weighted average method now exhibits peaks in the error that are two orders of magnitude smaller than before.
After the second refinement, instead, as in the vortex case, the errors in the conservation have grown significantly. Weighted average remains the technique with smaller values, while surprisingly, in this case the biggest oscillations are associated to the isoparametric approach.

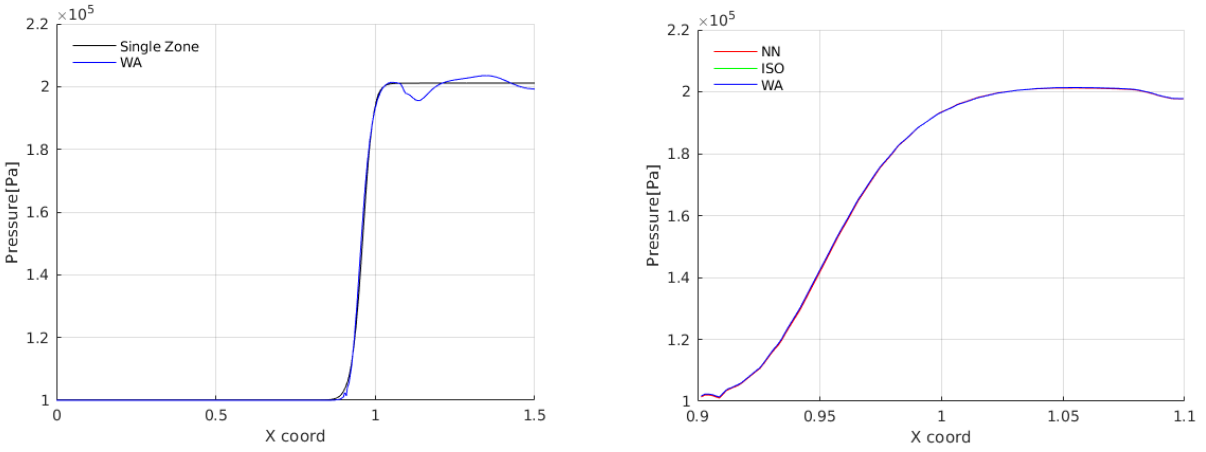

(a) Single Zone vs WA

(b) rotating zone

Figure 32: Oblique shock: The first picture shows the pressure profile obtained with the single zone simulation and weighted average. The pressure is plotted over an horizontal line that crosses the domain passing through the center of the internal zone. In the second plot, a close-up is provided for the internal zone to demonstrate that the difference between the three methods is nearly zero in terms of pressure.

After the computation of the conservation error, the analysis shifts its focus to the ability of these techniques to accurately compute flow properties. The following plots illustrate this point, taking the pressure before and after the shock wave as an example. In Fig. 32 is reported the pressure profile along a line crossing the domain from left to right, at constant $y = 0$.

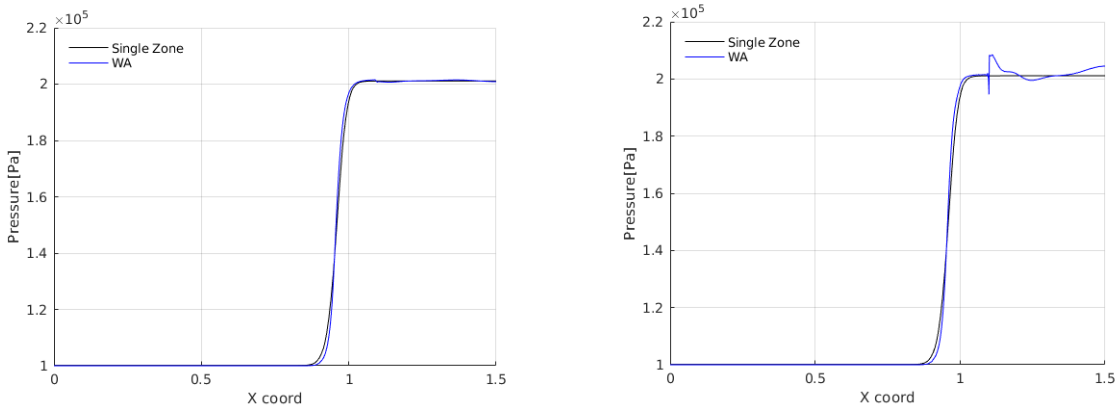

(a) Half size interface (b) One third interface

Figure 33: Oblique shock: The plots in this figure show the pressure profile in the case of half-size interface and one-third interface. The comparison is still made between the single zone results and the values obtained with the weighted average method.

In the first figure is clearly visible that pressure oscillations arise at the two extremes of the interface. The first oscillation, ahead of the shock wave, is pretty small; the second one instead, causes the pressure after the shock wave to drop about the 5% of its correct value. The perturbation generated at the interface is then propagated through the domain. The final results is that spurious oscillations are generated at the interface leading to a post-shock flow field with zones exhibiting higher pressure values and zones with lower ones.

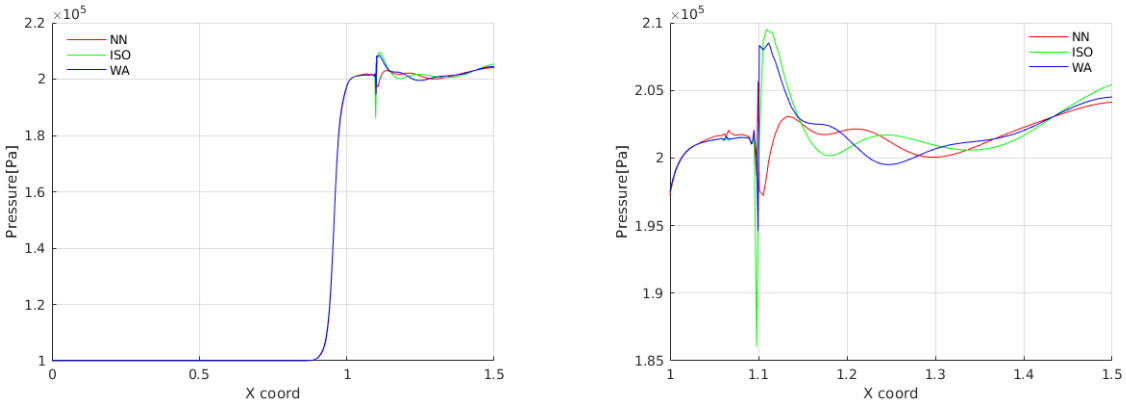

(a) One-third compare (b) Close up on the oscillations

Figure 34: Oblique shock: Comparison between the pressure profiles computed along an horizontal line intersecting the internal zone in its center. The profiles reported in the first figure are obtained with the three different approaches in the one-third scenario. The second one shows a close up on the oscillations to see the difference based on the method used.

As already noticed in the vortex advection case, despite the three methods having different mass conservation errors, the discrepancies in the flow properties, like the pressure, are almost zero. The refinement of the internal grid leads to significant changes in the results.
After the first refinement, i.e. with half-size interface, the pressure profile obtained in the multi-zone simulations gets really close to the reference one. Oscillations at the interfaces are still presents but they have no effect on the results. The small delay in the shock formation it's unavoidable, because this line crosses the shock wave in the internal zone, where the grid is half of the size of the reference one. These results are somewhat similar to those obtained in the vortex case, where the errors decreased with the first refinement. Once again, almost zero differences have been found between the three methods.
On the other hand, with the second refinement the situation get worse. The perturbations created drive the pressure far from the reference values, leading to a post-shock field similar to the same-size one. Surprisingly, in this case there are some differences between the pressure values obtained in the multi-zone simulations.

As depicted in Fig. 34 no differences can be found until the last interface cross. At that point the perturbations in the pressure values show up with different magnitude for every method. As expected from the trend of the conservation error the biggest deviation is associated to the isoparametric method.

8. Conclusions

In this paper, three different methods used to deal with non-conformal sliding mesh have been tested on a circular interface. The results obtained from all the conducted tests indicated that none of these methods proved to be conservative. Errors in the conservation of mass and total energy appear as soon as one of the zone is set to rotate.
These errors become worse if the complexity of the flow field is increased. Furthermore, the three methods yielded different error values, with differences that can be as large as two orders of magnitude. The errors in the conservation is found to depend on the grid size difference. The discrepancies between the Nearest Neighbor and the other two approaches can be reduced with the refinement of the donor zone. If instead only the target zone is refined, this difference increase, with Nearest Neighbor yielding the largest error.
Despite the conservation errors being relatively small, the sliding mesh techniques introduce oscillations that are then propagated into the domain. As observed in the vortex case, these effects can be reduced by using a lower time step; however, this comes at the cost of significantly increasing computational time. In the single zone simulations though, the vortex properties are very well conserved using the larger time step. To achieve comparable results, the multi-zone simulations instead, needed a ten time smaller time step. If the same time step value is used instead, conservation is not achieved from every perspective.
So in order to improve the computational capabilities of SU2 one potential future development could be the implementation of an interpolation-free technique, capable of achieving conservation and being independent on the relative displacement between adjacent zones.

References

[1] F. C. Dougherty J. A. Benek, J. L. Steger. A flexible grid embedding technique with application to the euler equations. *AIAA paper 83-1944*, 1983.

[2] J. L. Steger J. A. Benek, P. G. Buning. A 3-d chimera grid embedding technique. *AIAA paper 85-1523*, 1985.

[3] M. J. Berger. On conservation at grid interfaces. *SIAM J. Numer. Anal.*, 24:967–984, 1987.

[4] M. Rai. A conservative treatment of zonal boundaries for euler equation calculations. *J. Comput. Phys.*, 62:472–503, 1986.

[5] Z. N. Wu A. Lerat. Stable conservative multidomain treatments for implicit euler solvers. *J. Comput. Phys.*, 123:45–64, 1996.

[6] T. Tezduyar M. Behr. Shear-slip mesh update method. *Comput. Method Appl. M.*, 174:261–174, 2011.

[7] C. C. Pain G. J. Gorman C. R. Wilson P. E. Farrel, M. D. Piggott. Conservative interpolation between instructured meshes via supermesh construction. *Comput. Method. Appl. M.*, 198:2632–2642, 2009.

[8] R. Pecnik E. Rinaldi, P. Colonna. Flux conserving treatment of non conformal interfaces for finite-volume discretization of conservation laws. *Comput. fluids*, pages 126–139, 2015.

[9] G. Quaranta A. Guardone, D. Isola. Arbitrary lagrangian-eulerian formulation for two-dimensional flows using dynamic meshes with edge swapping. *J. Comput. Phys.*, 230:7706–7722, 2011.

[10] G. Quaranta D. Isola, A. Guardone. Finite-volume solution of two-dimensional compressible flows over dynamic adaptive grids. *J. Comput. Phys.*, 285:1–23, 2015.

[11] B. Re C. Dobrzynski and A. Guardone. An interpolation-free ale scheme for unsteady inviscid flows computations with large boundary displacements over three-dimensional adaptive grids. *J. Comput. Phys.*, 340:26–54, 2017.

[12] Sean R. Copeland Trent W. Lukaczyk Juan J. Alonso Thomas D. Economon, Francisco Palacios. Su2: An open-source suite for multiphysics simulation and design. *AIAA Journal*, 54:828–846, 2016.

[13] P.L. Roe. Approximate riemann solvers, parameter vectors and difference schemes. *J. Comput. Phys.*, 43:357–372, 1981.

[14] B. van Leer. Towards the ultimate conservative difference scheme. v. a second-order sequel to godunov's method. *J. Comput. Phys.*, 32:101–136, 1979.

[15] M. J. Djomehri H. C. Yee, N. D. Sandham. Low-dissipative high-order shock-capturing methods using characteristic-based filters. *Journal of Computational Physics*, 150:199–238, 1999.

[16] R. Duvigneau S. Pezzano. A fully-conservative sliding grid algorithm for compressible flows using an isogemoteric disconitnuous galerkin scheme. *Computer methods in applied mechanics and engineering*, 395, 2022.

[17] Philip A. Thompson. *compressible-fluid dynamics*. McGraw-Hill Inc., 1998.

[18] W. Speares E.F. Toro, M. Spruce. Restoration of the contact surface in the hll-riemann solver. *Shock Waves*, 4:25–34, 1994.

Abstract in lingua italiana

L'obiettivo della presente ricerca è analizzare se tre diverse tecniche numeriche utilizzate per gestire delle sliding mesh, nello specifico nearest neighbor, isoparametric e weighted average, possano introdurre errori nella conservazione delle proprietà del flusso quando si effettuano simulazioni con interfacce non rettilinee. L'analisi viene condotta confrontando tra di loro i tre approcci e valutando l'influenza del tipo di discretizzazione della griglia sugli errori di conservazione. A tale scopo, vengono esaminati quattro casi diversi con crescente complessità del campo di moto, partendo da un flusso uniforme e terminando con un flusso che presenta discontinuità come un'onda d'urto. La performance di queste tecniche verrà quindi valutata verificando sia la conservazione globale delle variabili conservative che la capacità di queste tecniche di preservare le caratteristiche del flusso. Nessuna di queste tre tecniche si è rivelata conservativa in quanto nè la massa nè l'energia totale nel dominio si conservano. L'effetto della non conservazione è l'introduzione di oscillazioni spurie delle variabili del flusso all'interfaccia che vengono poi propagated nel resto del dominio.

Parole chiave: sliding mesh, griglie non conformi, interfacce non rettilinee, metodo a volumi finiti non strutturati